A 2000-year temperature reconstruction on the East Antarctic plateau, from argon-nitrogen and water stable isotopes in the Aurora Basin North ice core.

Aymeric P. M. Servettaz[1,2], Anaïs J. Orsi[1,3], Mark A. J. Curran[4,5], Andrew D. Moy[4,5], Amaelle Landais[1], Joseph R. McConnell[6], Trevor J. Popp[7], Emmanuel Le Meur[8], Xavier Faïn[8], and Jérôme Chappelaz[8]

[1]Laboratoire des Sciences du Climat et de l'Environnement, LSCE/IPSL, CEA-CNRS-UVSQ, Université Paris-Saclay, Gif-sur-Yvette, 91190, France
[2]Biogeochemistry Research Center, Japan Agency for Marine-Earth Science and Technology, Yokosuka, 237-0061, Japan
[3]Department of Earth, Ocean and Atmospheric Sciences, University of British Columbia, Vancouver, V6T 1Z4, British Columbia, Canada
[4]Australian Antarctic Division, Kingston, 7050, Tasmania, Australia
[5]Antarctic Climate and Ecosystems Cooperative Research Centre, University of Tasmania, Hobart, 7000, Tasmania, Australia
[6]Division of Hydrologic Sciences, Desert Research Institute, Reno, 89512, Nevada, USA
[7]Niels Bohr Institute, University of Copenhagen, Copenhagen, 2200, Denmark
[8]University Grenoble Alpes, CNRS, IRD, Grenoble INP, IGE, 38000 Grenoble, France

Correspondence to: Aymeric P. M. Servettaz (servettaza@jamstec.go.jp)

Abstract. The temperature of the earth is one of the most important climate parameters. Proxy records of past climate changes, in particular temperature, are a fundamental tool for exploring internal climate processes and natural climate forcings. Despite the excellent information provided by ice core records in Antarctica, the temperature variability of the past 2000 years is difficult to evaluate from the low accumulation sites in the Antarctic continent interior. Here we present the results from the Aurora Basin North (ABN) ice core (71° S, 111° E, 2690 m a.s.l.) in the lower part of the East Antarctic plateau where accumulation is substantially higher than other ice core drilling sites on the plateau, and provide unprecedented insight in East Antarctic past temperature variability. We reconstructed the temperature of the last 2000 years using two independent methods: the widely used water stable isotopes ($\delta^{18}O$), and by inverse modelling of borehole temperature and past temperature gradients estimated from the inert gas stable isotopes ($\delta^{40}Ar$ and $\delta^{15}N$). This second reconstruction is based on three independent measurement types: borehole temperature, firn thickness, and firn temperature gradient. The $\delta^{18}O$ temperature reconstruction supports stable temperature conditions within 1°C over the past 2000 years, in agreement with other ice core $\delta^{18}O$ records in the region. However, the gas and borehole temperature reconstruction suggest that surface conditions 2°C cooler than average prevailed in the 1000–1400 CE period, and support a 20th century warming of 1°C. These changes are remarkably consistent with reconstructed Southern Annular Mode (SAM) variability, as it shows colder temperatures during the positive phase of the SAM in the beginning of the last millennium, with rapidly increasing temperature as the SAM changes to the negative phase. The transition to a negative SAM phase after 1400 CE is however not accompanied by a warming in West Antarctica, which suggests an influence of Pacific South American modes, inducing a cooling in West Antarctica while ABN is warming

**Climate
of the Past**

Discussions

Open Access

EGU

35   after this time. A precipitation hiatus during cold periods could explain why water isotope temperature reconstruction underestimates the temperature changes. Both reconstructions arguably record climate in their own way, with a focus on atmospheric and hydrologic cycles for water isotopes, as opposed to surface temperature for gases isotopes and borehole. This study demonstrates the importance of using a variety of sources for comprehensive paleoclimate reconstructions.

40   **Key Points:**

- Temperature reconstructions from water isotopes and borehole plus gas isotopes from the same ice core East Antarctica give substantially different climate histories for the past 2000 years.
- Water isotopes show low centennial variability, similarly to other East Antarctic Plateau ice cores; Borehole temperature and gas isotopes suggest a 2°C cooler 1000–1400 CE period, consistent with Southern Annular Mode
45   variability, as well as a 20th century warming of +1°C
- Differences emerge from the acquisition of temperature signal in the proxies, both spatially (atmosphere vs surface snow) and temporally (precipitation events vs diffusion over a few decades)

1 Introduction

The Antarctic continent is the only region where the recent warming trend cannot be distinguished from the high natural
50   climate variability (Abram et al., 2016). The sparse continuous measurements and the short timeframe covered by satellite era are insufficient to fully represent the climate in the vast continent that is Antarctica, and current climate models do not represent the full range of natural variability, highlighting that processes involved in the natural variability of temperature are still unclear (Jones et al., 2016). Therefore, climate archives such as ice cores can provide valuable information and help track the past evolution of temperature and climate (e.g., Jouzel et al., 2007; Stenni et al., 2017, among others). Understanding the
55   temperature variability in this ice-covered continent can improve the modelling of ice dynamics, melt events in coastal regions, predictions of ice sheet stability and the contribution to sea level rise, and is thus of critical importance when evaluating the risks associated with ongoing climate change (Meredith et al., 2022; Stokes et al., 2022).

The evolution of temperature during the last 2000 years is especially important as it provides a context of natural climate variability on timescales comparable to the recent warming, and temperature information is relatively well preserved in climate
60   proxies. Reviews of available temperature reconstructions were detailed for land (PAGES 2k Consortium, 2013) and oceans (Tierney et al., 2015). In Antarctica, the trends of different sub-regions for the past 2000 years were evaluated from temperature reconstructions based on water isotopes ($\delta^{18}O$ or δD) in ice cores, showing a general cooling (Stenni et al., 2017). The recent warming over the last 100 years is however not perceptible in all parts of Antarctica, resulting in an absence of significant warming for the continent as a whole. Ice cores included in the database used by Stenni et al., (2017) are unevenly spatially
65   distributed, especially the records covering the full 2000-year period, as ice cores are often drilled on domes or divides to avoid the glaciological advection of ice, leaving a vast gap of undocumented areas between coastal domes and the plateau summits.

In particular, the East Antarctic plateau temperature reconstructions are limited by low temporal resolution caused by the low accumulation in the dry high-elevation sites. In addition, most temperature reconstructions in Antarctica rely on water-stable isotopes, which could be seasonally biased (Werner et al., 2000; Persson et al., 2011), or altered by post-deposition effects (Landais et al., 2017; Casado et al., 2018). The regional climate would be better understood with temperature records from new locations, to increase the spatial coverage, and more diverse temperature proxies (Christiansen and Ljungqvist, 2017).

Studies of temperature variability in Antarctica have relied on temperature proxies from ice cores, especially water stable isotopes. The water stable isotopes measured in ice cores can be used to infer past temperatures, due to the relationship between cloud temperature and isotope composition of the precipitation: heavy isotopes in the atmospheric air mass are progressively flushed away as water condensates and precipitates (Dansgaard, 1964). Approaches to calibrate the isotope – temperature slope include: linear regression in the recent period when both temperature measurements and isotope records overlap (McMorrow et al., 2004; Steen-Larsen et al., 2014; Stenni et al., 2016; Casado et al., 2018), unidimensional isotope models (Ciais and Jouzel, 1994; Markle and Steig, 2022), or isotope-enabled general circulation model (Stenni et al., 2017; Goursaud et al., 2018). Even so, the slope calibrated over short periods may not transfer well to quantify the temperature variability at longer timescales (Jouzel et al., 2003; Casado et al., 2017), which is why the isotope – temperature slope should be carefully calibrated as close as possible as the expected variability (Jones et al., 2009).

Alternative solutions to reconstruct past temperatures have relied on the diffusion properties of temperature in the ice. Indeed, temperature of the ice is controlled by thermal diffusion and advection between the bedrock and the ice surface in contact with the atmosphere (Ritz, 1987). The bedrock-ice interface temperature, which depends on geothermal heat flux, is relatively stable at the timescales of a few thousands of years. Therefore, the atmosphere-surface snow temperature is the main source of variation in the ice temperature profile. This profile of temperature can be directly measured in the borehole after an ice core has been drilled, and can then be used to infer past surface temperature changes, using inverse methods and diffusion models with known heat diffusion properties in the ice (e.g., Johnsen et al., 1995; Dahl-Jensen et al., 1998; Orsi et al., 2012).

Finally, it is possible to assess the past temperature gradients from the diffusion of inert gases in the firn. The firn is the porous layer of compacted snow at the top of the ice sheet, which allows for movement of gases, mainly by diffusion. The diffusion of the isotopes of inert gases differs because of their physical properties, with primary control by gravitational settling of heavy gases at the bottom of the diffusive column (Craig et al., 1988; Sowers et al., 1992). In addition, a temperature difference between the two ends of the diffusive column can create an isotopic signal that can then be captured in the air bubbles trapped in the ice matrix (Severinghaus et al., 2001). The diffusive zone of the firn gases lies between the convective zone above, where gases are actively mixed by surface winds (Kawamura et al., 2013) or pressure changes (Buizert and Severinghaus, 2016), and a lock-in depth below, where the ice layers that merged under increased pressure block the vertical movement of gases (Buizert et al., 2012; Fourteau et al., 2019). Further below is the close-off depth where porosity is fully sealed, and gases are trapped in bubbles enclosed within an ice matrix (Severinghaus and Battle, 2006). The analysis of inert gas isotopes can thus be used to infer the past temperature gradients in the diffusive column of the firn (Kobashi et al., 2008). Reconstruction of temperature changes at the surface requires a thorough understanding of the vertical profile of temperature in the ice and

can be achieved by inverse modelling of a vertical temperature diffusion model in the firn (Orsi et al., 2014). Inversion of past temperature gradients estimated from gases isotopes has been applied in Greenland (Kobashi et al., 2008; Orsi et al., 2014), and some places in Antarctica (Orsi, 2013; Morgan et al., 2022), but remains rare compared to temperature reconstructions based on water isotopes, given the longer processing time, the volume of ice needed, and the analytical precision required in

105   inert gas analyses. Moreover, the accumulation rate controls the gases bubble enclosure speed, and restricts the locations where this method can be used to infer temperature changes: a too slow accumulation rate lets the time to the gases to diffuse out the temperature signals, while a too fast accumulation rate does not let the time for the gases to equilibrate with the firn, which is why this method is best used at sites within a 60–300 kg m^{-2} yr^{-1} accumulation range.

In short, the current temperature estimations for the East Antarctic Plateau are hindered by the low temporal resolution of ice

110   cores drilled in this region, which can be limiting to clearly assess the trends and variability at a sub-millennial timescale because of deposition dynamics and post-deposition processes masking the climate signal (Münch and Laepple, 2018; Casado et al., 2020). Moreover, the large majority of temperature reconstructions rely on water stable isotopes, in a region where ice accumulation is uneven through time (Turner et al., 2019) and may induce biases in water isotopes based reconstructions. In this study, we try to address both issues by reconstructing the temperature from the Aurora Basin North ice core with two

115   independent methods. We first use the water stable isotopes and expect that the relatively high ice accumulation for a Plateau site, of about 100 kg m^{-2} yr^{-1} (Akers et al., 2022), will result in a more detailed temporal resolution and may better record the centennial variability of East Antarctic Plateau temperatures. Then, we use gases isotopes and borehole thermometry in an inverse model to retrieve surface temperature changes. We finally compare the two reconstructions and discuss the climate implications along with other Antarctic records.

120   ## 2 Material and methods

2.1 Aurora Basin North site description

Aurora Basin North (ABN) is located inland East Antarctica, at 71.17° S, 111.37° E at 2,690 m elevation. The ABN site is approximately mid-distance between the coast and Dome C, on the Indian Ocean sector (Fig. 1). This site is located on the East Antarctic plateau, but much closer to the ocean and thus receives significantly more snowfall than EPICA Dome C or

125   Vostok, making it more suited for studies of the late Holocene climate, with a water isotope record resolved at a near annual scale (Moy et al., 2017). The 20th century snow accumulation at ABN is estimated at 126 ± 26 kg m^2 yr^{-1}, up from the 94 ± 18 kg m^2 yr^{-1} before 1900 CE (Akers et al., 2022). The temperature at ABN shows a high positive correlation with a large part of the Indian sector of continental East Antarctica at interannual scale, as estimated from a regional atmospheric model (Servettaz et al., 2020). A 303 m core was drilled at ABN in the summer of 2013–2014, named ABN1314, which is used in

130   this study. Additionally, we use data from a 12 m shallow firn core to cover the most recent snow (described in Servettaz et al., 2020).
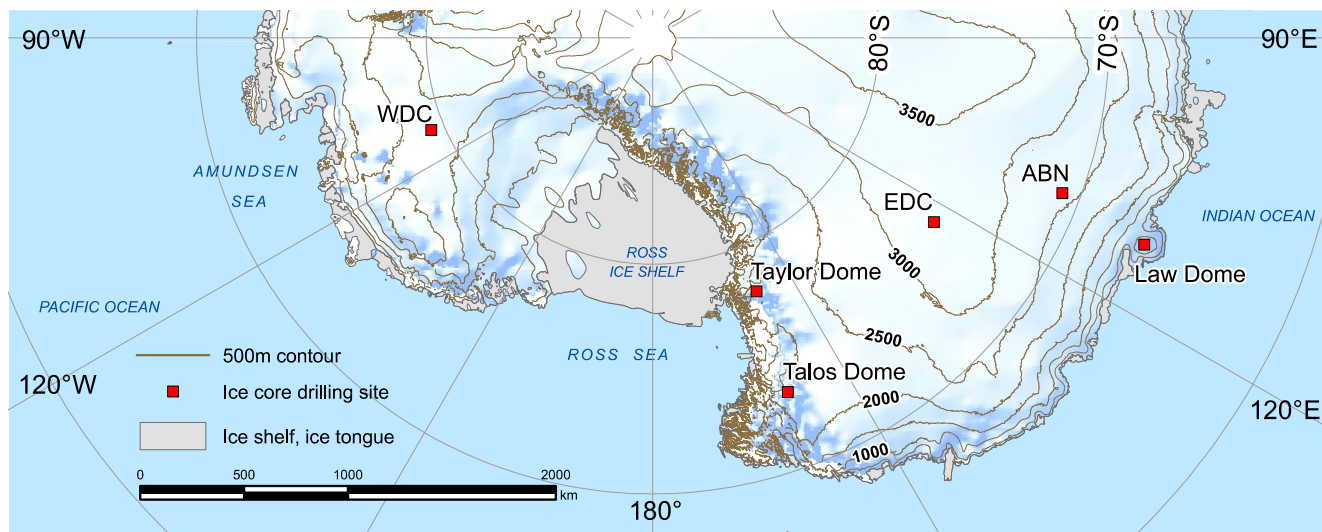
Figure 1. Map of the Indian and Pacific sectors of Antarctica. A selection of ice core drilling sites is shown: ABN – Aurora Basin North (this study), Law Dome, EDC – EPICA Dome C, WDC – West Antarctic Ice Sheet Divide Core, Talos Dome, Taylor Dome.
135   **True scale at 71° S. Modified from a production of the Australian Antarctic Data Centre, June 2009 (map catalogue no. 13641 – data.aad.gov.au © Commonwealth of Australia 2009). Creative Commons Attribution 4.0 Unported License.**

2.2 Measurements

2.2.1 Water stable isotopes

The ABN1314 core was subsampled at 20 cm resolution for water stable isotope analysis at the Australian Antarctic Division.
140   Water stable isotopes (δ^{18}O and δD) analysis were performed on a Picarro L2130-i isotopic water analyser. Aliquots of water were sampled by a Picarro liquid auto-sampler and injected into a Picarro high precision vaporization module (A0211) and held at temperature of 110°C with the vapour sent to the Picarro L2130-i isotopic water analyser. Isotopic values are expressed as per mil (‰) and relative to the Vienna Standard Mean Oceanic Water (V-SMOW) standard. The standard deviation of the δ^{18}O values for repeated measurements of laboratory reference water samples was less than 0.05 ‰ and less than 0.5 ‰ for
145   δD. A total of 1522 measurements were performed on the 303 m core. Although δ^{18}O and δD are roughly proportional, deviation from the standard meteoric water line likely results from changes in the evaporation conditions at the moisture source (Dansgaard, 1964; Uemura et al., 2008). The deviation from the meteoric water line can be defined with a logarithmic notation (Uemura et al., 2012):

$$d_{\ln} = 1,000 \times \ln(1 + \delta D) + 2.85.10^{-2} \times \left(1,000 \times \ln(1 + \delta^{18}O)\right)^2 - 8.47 \times 1,000 \times \ln(1 + \delta^{18}O) \qquad (1)$$

150   The propagated uncertainty gives an analytical precision for $d_{\ln}$ of 0.52 ‰.

2.2.2 Gases stable isotopes

Gas-dedicated samples of about 20 cm in length were subsampled approximately every 2 m in the ABN1314 core. Due to the porosity of the ice sheet, gas samples were taken below the lock-in depth, starting at 104 m depth. The samples' outer ice was

shaved off to prevent contamination by exchange with air during transport and storage, and each sample was split into two

155 duplicates of ~70 g each.

In order to measure precise argon isotopes, O_2 was removed due to isobaric interference between ^{36}Ar and $^{18}O^{18}O$. Argon and nitrogen gases were extracted from the ice following the method of (Kobashi et al., 2008): the ice was melted in a pre-emptively evacuated bottle, and the gases were released in a processing line with cold traps to remove water vapour and carbon dioxide, and then uses a heated copper mesh (500°C) to remove molecular oxygen. The remaining gases are trapped in a collection tube

160 that is cooled with liquid helium. To maximize the efficiency of the traps, the gases were released slowly in the processing line, with the pressure in the collection tube maintained under 50 Pa at all times. Once the entirety of the gases was released into the processing line, the collection continued for about 15 minutes, until the pressure drops under $5 \cdot 10^{-2}$ Pa, to ensure complete trapping of the gases. The collected gases are left to heat up to room temperature and homogenise in the collection tube overnight, and then measured on a dual inlet mass spectrometer (MAT 253+) against a laboratory standard of N_2, Ar, Kr.

165 The MAT 253+ spectrometer was setup so that different isotopes of a same element are measured simultaneously in an arrangement of collection cups dedicated to N_2, Ar, or Kr. The standard is calibrated weekly against modern air following the same protocol as the ice sample, from release in the processing line to mass spectrometry.

We use the $\delta^{40}Ar$ and $\delta^{15}N$ notations for isotopic ratios $^{40}Ar/^{36}Ar$ and $^{15}N/^{14}N$ in the sample relative to the isotopic ratios in the free atmosphere (IAEA, 1995). The dual inlet system that sends gas to the spectrometer switches between the sample and

170 laboratory standard in cycles for robust measurement of the isotopic ratio. Cycles of 11 standard and 10 sample injections were repeated 5 times with the spectrometer in argon configuration and 3 times in nitrogen configuration. Additionally, elemental ratios were measured following the peak-jumping method (Bereiter et al., 2018).

Pressure imbalance and chemical slope corrections were applied to account for the imbalance in the dual inlet system and the elemental ratios in the sample, first described by Severinghaus et al. (2003; details of the corrections used in this study are

175 given in Appendix A3). In addition to the previously described corrections, it was identified that the spectrometer focus drifted over time, that resulted in a strong variability of both $\delta^{40}Ar$ and the value used pressure imbalance correction. While the measurements took about nine months to complete, the pressure imbalance correction value was verified daily, and estimates of the intensity of $\delta^{40}Ar$ error resulting from the spectrometer focus were made using the daily value of pressure imbalance correction, which is itself dependant on spectrometer parameters. We thus corrected for the spectrometer drift (details of this

180 correction are given in Appendix A3). This drift correction halved the pooled standard deviation of $\delta^{40}Ar$ in the ice duplicates. While Kobashi et al. (2008) have reported argon loss during storage of ice for extended amount of time at a temperature of −20°C, the excellent quality of ice from a recently drilled ice core, and the precautions taken during the preparation prevented any notable effect of argon loss during storage on the $\delta^{40}Ar$ measured in our samples.

A total of 102 pairs of duplicates were analysed, and this was complemented by three single samples that could not be

185 duplicated because they were taken from ice samples that were too small to be split in two, or for which one sample of the duplicate pair was lost due to a leak during processing. Given ice samples were processed in duplicates and have undergone the same procedure, we evaluate the reproducibility of the method and analysis by comparing duplicate results. The pooled

standard deviation of the 102 duplicates is 0.0159 ‰ for $\delta^{40}Ar$ and 0.0045 ‰ for $\delta^{15}N$. Three samples had exceptionally high duplicate differences, with higher than three times the pooled standard deviation for either $\delta^{40}Ar$ or $\delta^{15}N$. These samples had

190   been flagged as potentially contaminated due to a change of operator and an unplanned power outage during processing. Another four shallow duplicates, taken just below the close-off depth, had $\delta^{40}Ar$ and $\delta^{15}N$ values significantly lower than the gases in the open porosity of the lock-in depth above. At ABN, the close-off depth of ~104 m below surface is where the pores are completely closed, and the air bubbles are trapped in an ice matrix. Recent bubbles in the ice around this depth were probably thinly closed at the time of sampling and may have been contaminated with more recent air before the pores were

195   fully sealed. Another possibility is that vacuum pumping on thinly closed porosity may have altered the isotopic composition during gas sample preparation. These samples were considered as outliers and will not be included in the final dataset, which consists of 95 duplicates and 3 singletons. After removal of outliers, the pooled standard deviation of remaining samples is 0.0137 ‰ for $\delta^{40}Ar$ and 0.0036 ‰ for $\delta^{15}N$.

The bubble trapping was shown to be heterogeneous at the 10 cm scale, causing variability in the isotopic composition of the

200   gases (Orsi, 2013), probably because of the differential closure rate of bubbles in summer versus winter layers of ice (Severinghaus and Battle, 2006). Due to the high frequency variability of gases, the isotopic composition cannot be related to climate information. The data is thus smoothed by resampling using a 5 m window to average both $\delta^{15}N$ and $\delta^{40}Ar$ (Fig. 2). The uncertainty on the resampled points was inferred as the standard deviation of all points in the 5 m window. Hereafter in this study, the smoothed data with a 5 m resolution is used.
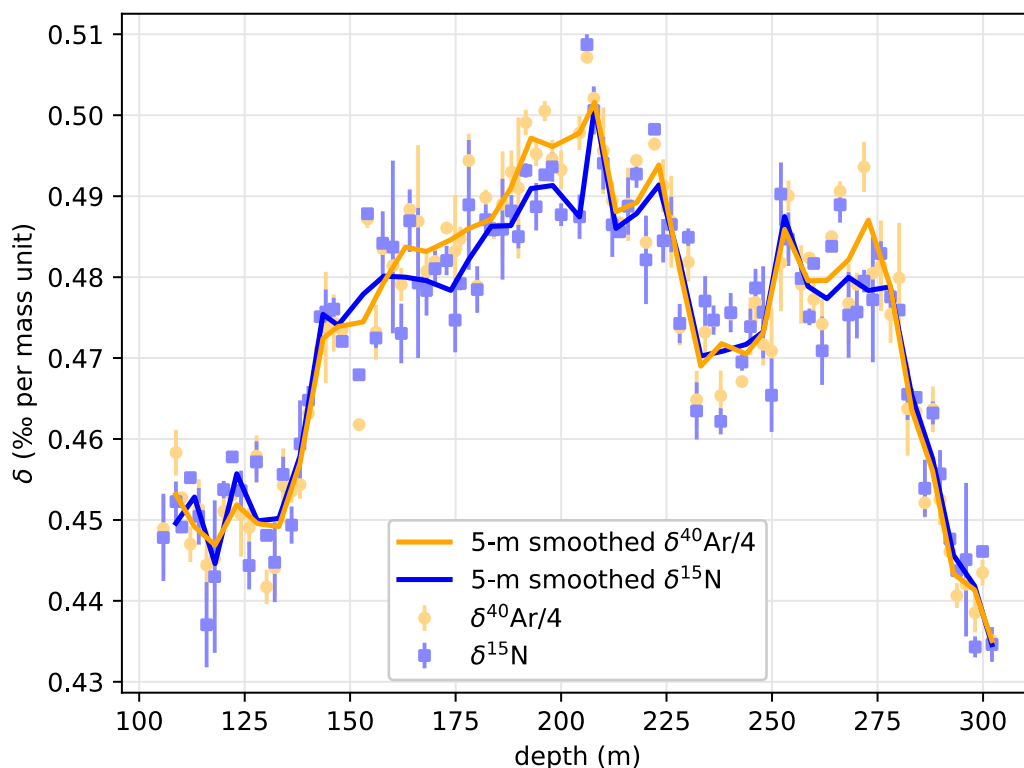
Figure 2. Series of δ⁴⁰Ar (orange) and δ¹⁵N (blue) in the ABN1314 core. Large dots and squares represent the average value for a given depth, error bars illustrate the difference between duplicates. The 5 m smoothing is shown with solid lines for both series.
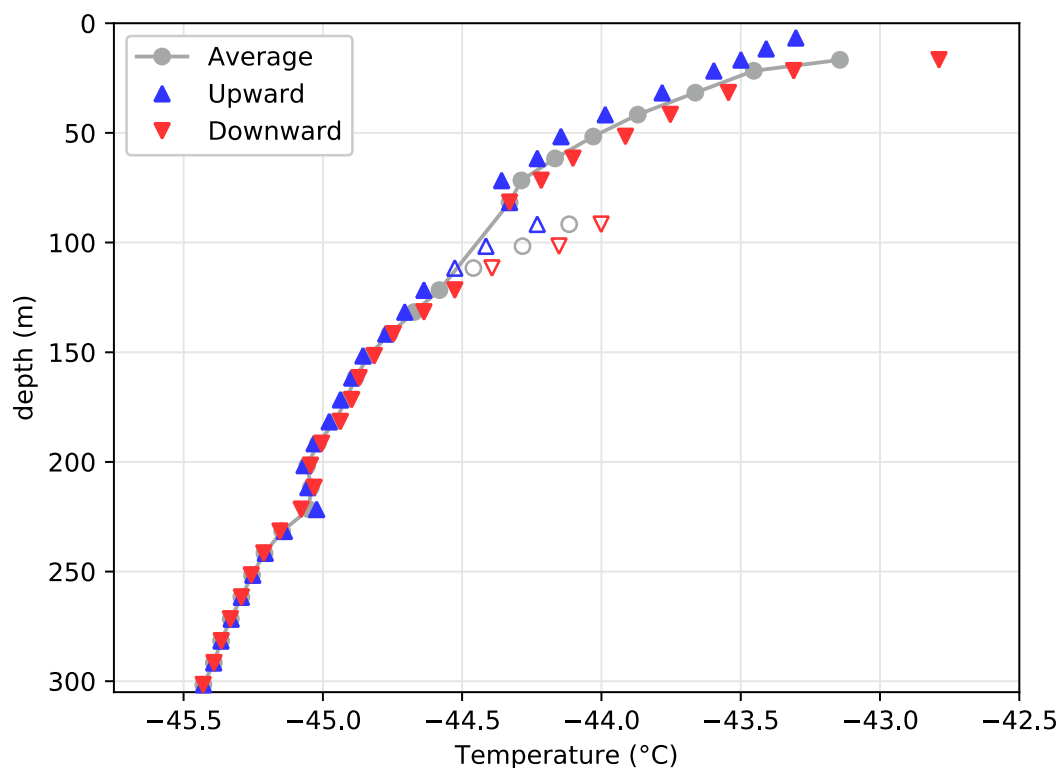
2.2.3 Borehole temperature

The Borehole temperature measurements were made by lowering a measuring resistor with a three-bladed probe down the borehole. The resistance was measured using a Fluke multimeter, and converted to temperature using temperature dependence of resistivity. The probe was stopped at target depths and let equilibrate with surrounding ice until a stable measurement could be achieved. A second series of measurements was made at the same depths when the probe was pulled back up, providing two temperature values for each depth (downward and upward, Fig. 3). Wet drilling (Estisol) commenced from 132 m, and it is very likely that the open markers in Fig. 3 are outliers due to disturbance of air in the drill hole with warm fluid stored at the surface. Below 132 m, the small difference between upward and downward measurements is likely due to improved equilibrium in the drilling fluid. Relatively short equilibrium time before each measurement may have caused the downward temperature to be overestimated whilst the upward temperature series is underestimated because of the memory effect of the temperature probe, particularly above the drilling fluid. Even though the temperature was measured only few weeks after the drilling had completed, the heating effect of the drilling is relatively small, estimated at ~0.1°C (Orsi et al., 2017). The

220   temperature measured ranged from –45.5°C at the bottom of the drill hole to –43.1°C at 17 m below the surface, deep enough

for the temperature not to be affected by seasonal variations, revealing a gradient larger than 2°C over the 300 m depth.

Figure 3. Temperature profile in the Aurora Basin North main core borehole. The drilling fluid may have induced a disturbance of air temperature in the drill hole because the drilling fluid was stored at the surface at a warmer temperature of about −20°C. Open
225   **markers indicate points that will be ignored for this reason. Below 132 m, the small difference between upward and downward measurements is likely due to improved equilibrium in the drilling fluid.**

2.3 Ice core age model

2.3.1 Ice age model

Producing a well-constrained age model is a necessary step in the analysis of a paleoclimate record. Chemical species, electro-
230   conductivity, and water stable isotopes were measured at high resolution with Continuous Flow Analysis (CFA) at the Desert

Research Institute (Maselli et al., 2013; McConnell et al., 2002), allowed identification of annual cycles in most of the

ABN1314 ice core. The ABN1314 core was dated by Annual Layer Counting (ALC) of seasonally varying aerosols (Na^+, Cl),

electro-conductivity and water isotope measurements. The ALC was performed manually and subsequently tied to volcanic

events using sulphate aerosols from other well dated ice core records. The ABN1314 total sulphur record was compared to the
235   Plateau Remote (Cole-Dai et al., 2000) and West Antarctic Ice Sheet Divide (Sigl et al., 2013) ice cores, as all sites are inland

Climate
of the Past
Discussions

Antarctica and have similar backgrounds for sulphur. Even though Law Dome is the nearest site with high resolution sulphur record, the background is very different, likely due to Law Dome being a coastal site. ALC was adjusted using 29 volcanic horizons that were matched to the WD2014 chronology (Sigl et al., 2016). The surface snow mixing by wind at ABN is of comparable scale with the yearly accumulation (up to 40 cm of snow, Servettaz et al., 2020), which may have hindered the

240   identification of annual signals used for year identification in ALC especially during periods of lower accumulation. Therefore, the ABN1314 ALC was anchored to the WD2014 chronology with volcanic ties, and then ALC was performed a second time in between ties to find the expected number of years. The uncertainty on the age of volcanic horizons in the WD2014 chronology is lower than 5 years, and hence we report all the volcanic ties with a ± 5-year margin to account for this uncertainty. The ABN1314 core covers the last 2700 years (Fig. 4). Dating uncertainties resulting from the ALC were considered as follows:

245   if an annual layer was counted but is not on a clear seasonal extremum, it is flagged as uncertain, and a half-year uncertainty is added (details on the uncertainty is shown in Fig. A1). The age model for the ABN1314 core is referred to as ALC-01-11-2018. Through the volcanic age tying, the age model for ABN1314 has consistently low uncertainties of less than 20 years.
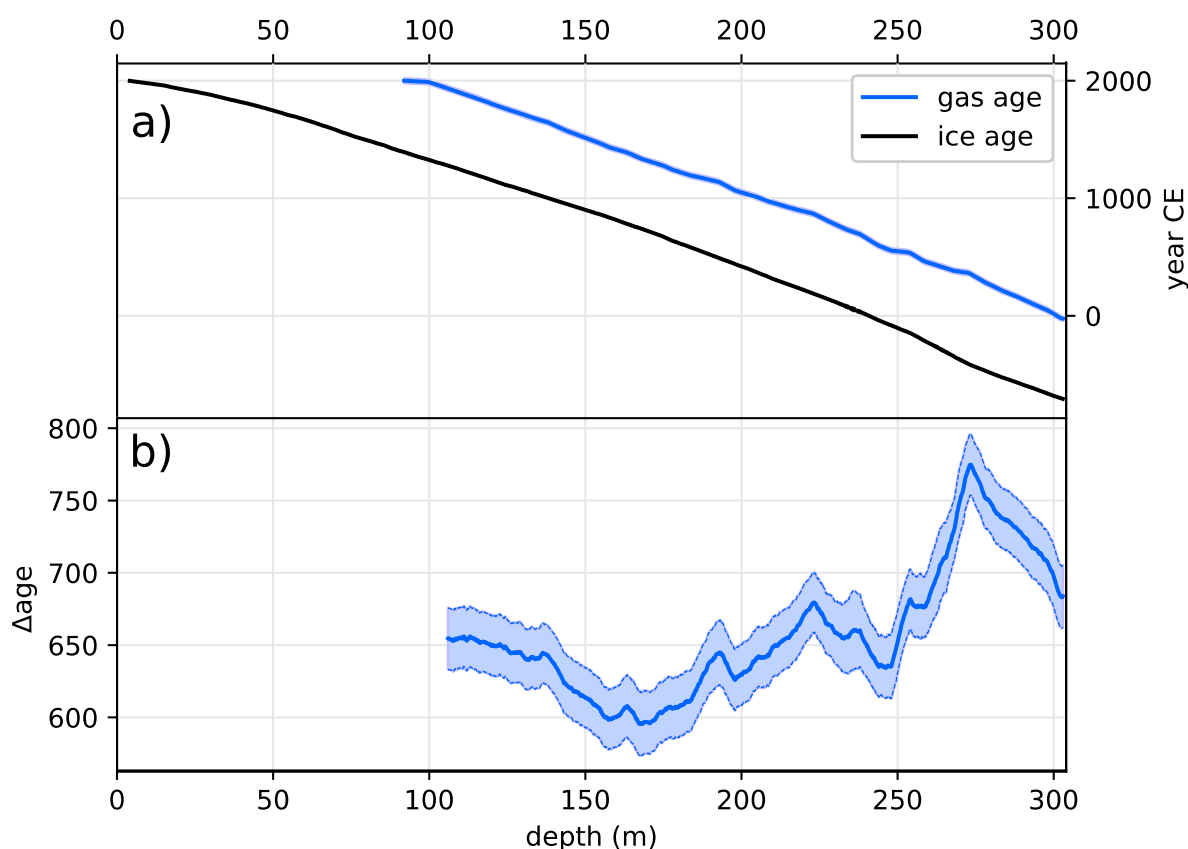
Figure 4. (a) Ice and gas age models for the ABN1314 ice core. The ice age model is based on Annual Layer Counting of seasonally

250   varying chemical species, while gas age model is based on methane ties. Both age models are tied to WD2014 chronology for ice and

gases respectively (Sigl et al., 2015a, 2016b). (b) Δage defined as the difference between ice and gas ages at each corresponding depth. Shading indicates the estimated uncertainty.

2.3.2 Gas age model

The gases are trapped by closure of the porosity at the bottom of the firn, and hence are enclosed in bubbles surrounded by
255 substantially older ice. Preliminary dating of the gases is completed by subtracting a constant age difference to the surrounding ice, corresponding to the modern-day difference between age of gases and ice at the lock-in depth. Firn characteristics may vary through time, affecting the height of the diffusive zone and thus the lock-in depth, and hence the gas age model is further refined with the methane record measured in the ABN1314 core.

The methane content of gases trapped in ABN1314 was measured with the Desert Research Institute Continuous Flow Analysis
260 system that was modified for gas measurement (Rhodes et al., 2013). We used methane records to tie gas ages scale of the ABN1314 core with the established chronology of the West Antarctic Ice Sheet (WAIS) Divide ice core, named WD2014 (Sigl et al., 2016). Specifically, we defined tied points so that the methane content in bubbles at ABN fits the published methane dataset from the West Antarctic Ice Sheet (WAIS) Divide ice core, named WD2014 (Sigl et al., 2016). Tie points were identified where there is clear, quick transitions or extrema on methane records (Fig. A2).

265 For the most recent part (1800 to 2000 CE, Fig. 4b), the methane data from WAIS Divide was not available, and hence the ABN methane record was tied to the revised Law Dome record (Rubino et al., 2019). Again, samples taken between above the close-off depth of ~104 m below surface, which corresponds to 1925 CE, are likely to be contaminated with recent air before the pores were sealed, resulting in higher methane concentrations.

The gases are younger than the ice at the same depth, so the gas age model of ABN1314 core only covers the last 2050 years.
270 The most recent gases are technically still in the diffusive column of the firn, or partly in the remaining open porosity between lock-in and close of depth, but not fully trapped in bubbles within an ice matrix. The uppermost ice core samples that contain gases suited for analyses are found below the close-off depth, dated to 1925 CE. Because the ages were tied manually, it is difficult to estimate the uncertainty, but the tie points used correspond to events with an age span shorter than 20 years. While the lock-in depth of gases may vary depending on the species due to diffusivity speed in the firn (Witrant et al., 2012), the
275 resulting difference is expected to be much lower than 20 years at ABN. Therefore, we roughly estimate the uncertainty on the gas age model to be 20 years.

2.3.3 Gas-ice age difference

The difference between gas age and ice age provides information on the dynamics of the firn and its evolution through time. A larger age difference may result from a decrease in accumulation rate or an increase of lock-in depth where gases are trapped.
280 Fig. 4 shows the gas and ice age models and the difference of age between gases and ice at a given depth. The gas-ice age difference is comprised between 600 and 700 years, except for one excursion at around 270 m depth which is likely related to

the sudden change of accumulation caused by a dune-like feature upstream from the ABN site, which was advected under the current ABN location with ice flow.

2.4 Ice flow correction

285 In opposition to many ice core drill sites that target a dome or a divide, ABN was drilled in a basin setting, where ice slowly flows from the continent to the coast. The estimated ice flow is determined by comparing the accumulation record from the ice age model, and the first isochron reflector depth from the ground penetrating radar survey upstream of ABN: the first order of accumulation changes is driven by local accumulation features caused by the topographic slope (Van Liefferinge et al., 2021; Akers et al., 2022). Indeed, the speed of the katabatic wind scales with terrain slope (Parish and Bromwich, 1991; Vihma

290 et al., 2011), and thus acceleration of wind scales with terrain curvature. Accelerating winds can charge up in snow particles and locally reduce the accumulation. Conversely, decelerating winds deposit the drifting snow, increasing the accumulation. By matching the time-series of accumulation from the ABN1314 core to the upstream accumulation patterns (Fig. A3), we estimate that the bottom part of the ABN ice core corresponds to ice originating 41.5 km upstream from the ABN drill site, which results in an average ice flow of 15.4 m yr^{-1}. This value is in relatively good agreement with satellite-based estimation

295 of 16.2 m yr^{-1} at ABN for the 1996–2018 period (Mouginot et al., 2019).
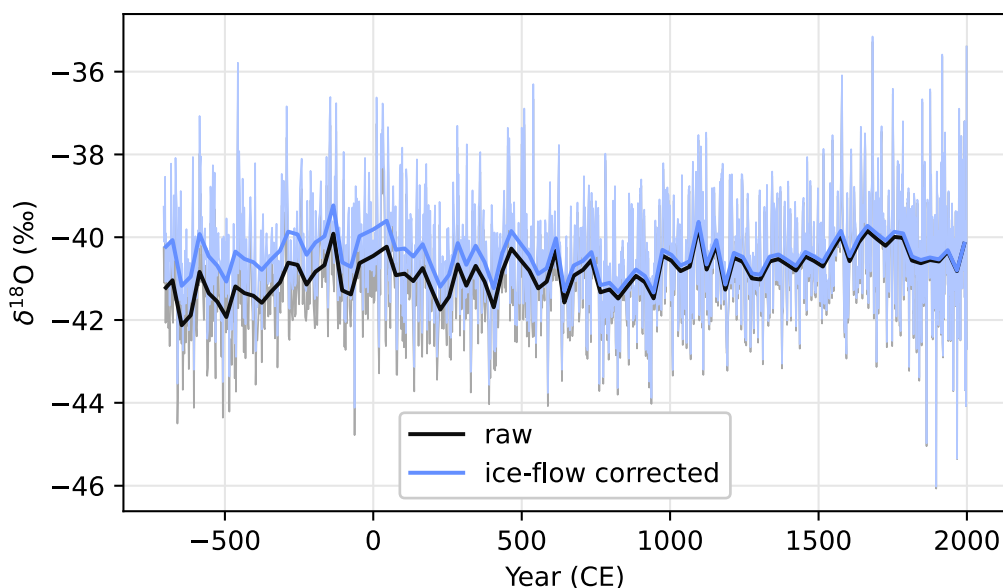

Figure 5. δ^{18}O in the ABN1314 ice core, with a sampling resolution of 20 cm (thin lines) and on 30-year average (Thick lines). The analytical uncertainties on δ^{18}O of 0.5 ‰ are not shown on the figure. Black lines show the raw measurement and blue lines show the glaciology-corrected values.

300 Using this ice flow velocity, the estimated origin altitude of the ice in the ABN1314 core, or the paleo-elevation of the ABN drilling site is made. The ice dating from 700 BCE was formed at an elevation of 2745 m, and subsequent ice forming the

ABN1314 ice core originated from lower elevation, down to the drill site at 2690 m for the most recent snow (Fig. A3). We estimated that a decrease of 55 m elevation would cause a temperature increase of 1°C, using the temperatures interpolated with kriging from Automatic Weather Stations and borehole temperature measurements for two traverses in nearby Princess Elizabeth Land, East Antarctica (Xiao et al., 2013; Pang et al., 2015; Fig. A4). The regression was performed on a subset of the traverse between 2000 and 3250 m above sea level, corresponding to the lower plateau around the elevation where ABN is located. Similarly for water stable isotopes, the estimated decrease of 55 m elevation would result in a δ^{18}O increase of about 1 ‰, by calibrating a δ^{18}O–elevation slope in surface snow studies at elevations comprised between 2000 and 3250 m above sea level, and longitudes from 80° E to 160° E (Xiao et al., 2013; Pang et al., 2015; Goursaud et al., 2018; Fig. A5). The measured δ^{18}O and ice-flow corrected δ^{18}O are shown on Fig. 5. We did not find any significant relationship between elevation and d_{ln} at this elevation range (Fig. A6), and therefore did not correct it for glacial flow.

3 Temperature reconstructions

3.1 Water stable isotopes

Water isotopes in ice cores have consistently been used to estimate past temperatures (e.g., Cuffey et al., 1995; Jouzel et al., 1997, 2003; Stenni et al., 2017). The ABN isotope record consists of 1522 data points for the 2707 years covered by the ice core, resulting in a temporal resolution of δ^{18}O slightly above one point for two years. However, the water isotopes are strongly affected by deposition variability and non-climatic factors that may mask the climate signal at high resolution, especially for regions such as the East Antarctic Plateau where the accumulation is low (Münch and Laepple, 2018; Casado et al., 2020). Moreover, a few extreme precipitation events can be responsible for a large part of the total yearly accumulation (Turner et al., 2019), so it is more reliable to average over several years to retrieve the climate information from the water isotope record. Therefore, a 30-year average is used to better determine the climate signal. The 30-year averaged δ^{18}O series has a mean value of -40.8 ± 0.5 ‰ (1σ) and shows minimal variation over time.

The ABN δ^{18}O – temperature slope is determined using the δ^{18}O record from the 12 m shallow core that is dated back to 1968. The shallow core overlaps the time period with the Modèle Atmosphérique Régional (MAR) modelled temperature on the 1979–2013 period (Agosta et al., 2019), and MAR was shown to model the surface temperature more accurately than any other available dataset when compared with automatic weather station observations near ABN (Servettaz et al., 2020). MAR is thus used as the temperature reference for ABN, because the nearest automatic weather station temperature data record (1985–1993) is too short to capture the interannual variability of temperature. We calibrate a δ^{18}O – temperature slope for ABN using linear regression on the 1991 to 2013 period, where we are confident on the dating and have a decent number of years. Both temperature and δ^{18}O are averaged annually to minimise the influence of seasonal variability.
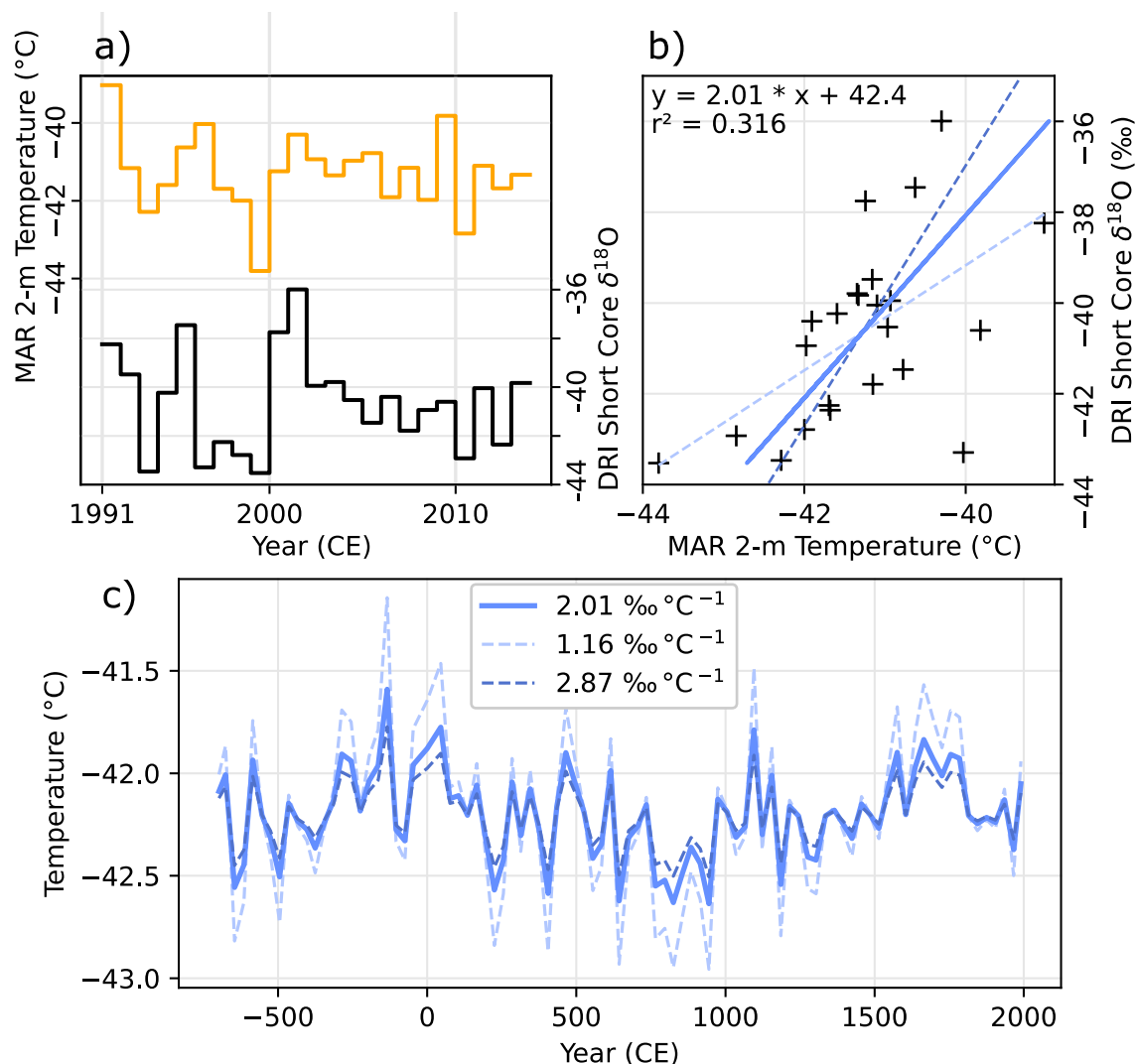
Figure 6. Calibration of δ¹⁸O – temperature slope with the Desert Research Institute (DRI) Short Core δ¹⁸O and the 2 m temperature in the Modèle Atmosphérique Régional (MAR) on the 1991–2013 CE period. (a) Annually averaged series of MAR 2 m temperature (orange) and DRI Short Core δ¹⁸O, on their overlapping period of 23 full years from 1991 to 2013. (b) Scatterplot of the two datasets (black crosses), with linear regression in blue solid line. Dashed lines represent the slope upper and lower uncertainties at a 95 % confidence level. (c) Temperature reconstruction using the δ¹⁸O series from the ABN1314 core and the slope obtained with linear regression, with temperature reconstructed with upper and lower uncertainty slope values in dashed lines.

We determine a $\delta^{18}O$ – temperature slope $\alpha = 2.01$ ‰ °C^{-1}, with a 95 % confidence interval of $1.16 < \alpha < 2.87$ ‰ °C^{-1}.

According to this slope, a change of 1°C in the mean annual temperature would be recorded in the snow by a ~2 ‰ change in $\delta^{18}O$. This 2.01 ‰ °C^{-1} slope is relatively high compared with other slope values estimated with ECHAM5-wiso, which average 1.00 ‰ °C^{-1} in East Antarctica (Stenni et al., 2017), or 0.85 ‰ °C^{-1} at ABN (Servettaz et al., 2020). This difference

14

could be at least partly attributed to the ECHAM5-wiso model, known to underestimate the inter-annual variability of isotopes in Antarctica (Goursaud et al., 2018).

345 Here, we use the 2.01 ‰ °C^{-1} slope to convert the δ^{18}O corrected for ice flow from ABN1314 to a reconstructed temperature record (Fig. 6c). The ice flow correction described in Sect. 2.4 is applied to the δ^{18}O data before converting it to a temperature record, to emulate a δ^{18}O record at the current ABN location. The δ^{18}O–temperature calibration slope was defined on a shorter period of 23 years that should not be affected by ice flow. The temperature obtained from this reconstruction averages −42.0°C and remained within a 1°C range (from −42.6 to −41.6°C) over the past 2700 years (Fig. 6). The use of a different δ^{18}O –

350 temperature slope slightly modifies the range of temperature values (Fig. 6c) but does not modify our interpretation. We acknowledge that using a δ^{18}O – temperature slope calibrated with yearly averages is not optimal given the limitations caused by deposition dynamics and post-deposition processes, but the δ^{18}O – temperature calibration is limited by the length of overlapping δ^{18}O and available temperature records. The temperature reconstruction from δ^{18}O at ABN might also be biased, as precipitations occur consistently during warm events (Servettaz et al., 2020).

355 **3.2 Gases and borehole temperature inversion**

While the water isotopes have been the proxy of choice for many paleoclimate studies in Antarctica, past temperatures are also imprinted in the ice and can be measured in the borehole after the ice core has been drilled. However, the temperature slowly diffuses in the ice, smoothing out the signal over time. Diverse inversion methods have been applied to estimate temperature changes since the last deglaciation (e.g., Dahl-Jensen et al., 1998) or over the last millennium (Orsi et al., 2012), but the

360 temperature reconstruction from borehole quickly loses temporal resolution over time. Another method to estimate past temperature changes relies on the thermal fractionation of gases in the firn diffusive column, where a gradient of temperature can be captured in the δ^{15}N and δ^{40}Ar composition of the air trapped in bubbles of the ice core (Kobashi et al., 2008; Orsi et al., 2014). Here, we also reconstruct past temperatures at ABN using a combination of the borehole temperature and the past temperature gradients estimated from gases isotopes.

365 **3.2.1 Determination of temperature profile and past temperature gradients**

The temperature profile was measured directly in the borehole after ice core was drilled. The temperature profile of ABN borehole (Fig. 3) shows a strong decrease of temperature at depth, suggesting that the surface warmed while old ice buried under remained colder. We observe a near-surface temperature gradient of ~1°C 100 m^{-1}, for which a 2.7°C warming over the last 30 years was inferred at a Greenland site (Orsi et al., 2017). On the East Antarctic Plateau however, no such warming

370 trend was previously detected (Nicolas and Bromwich, 2014). We expect that the ABN temperature gradient partly results from ice rheology, displacing the ice from a colder location upstream to what is now buried under ABN site.
Gravitational and thermal fractionation affect the gas contained in the firn porosity. The temperature gradient in the diffusive column controls the thermal fractionation, while the height of the diffusive column determines the gravitational fractionation.

Knowing the fractionation coefficients, we retrieve the temperature gradient (noted ΔT) of the firn at different times. The

375 gravitational effect on isotopes (noted δ_{grav}) is mass dependent, while the thermal fractionation can be approximated as a linear

function of the temperature gradient in the firn, with different fractionation coefficients for nitrogen (Ω_{15}) and argon (Ω_{40})

gases (Severinghaus et al., 2001). Gravitational and thermal effects on fractionation can thus be disentangled using two pair

of isotopes, as described by the following system:

$$\begin{cases} \delta^{15}N = \delta_{grav} + \Omega_{15} \cdot \Delta T \\ \delta^{40}Ar = 4 \cdot \delta_{grav} + \Omega_{40} \cdot \Delta T \end{cases} \tag{2}$$

380

So δ_{grav} and ΔT can be written as a function of $\delta^{15}N$ and $\delta^{40}Ar$:

$$\begin{cases} \Delta T = \dfrac{\delta^{15}N - \frac{1}{4} \cdot \delta^{40}Ar}{\Omega_{15} - \frac{1}{4} \cdot \Omega_{40}} = \dfrac{^{15}N_{excess}}{\Omega_{15} - \frac{1}{4} \cdot \Omega_{40}} \\ \delta_{grav} = \dfrac{\Omega_{15} \cdot \delta^{40}Ar - \Omega_{40} \cdot \delta^{15}N}{4\Omega_{15} - \Omega_{40}} \end{cases} \tag{3}$$

We use the Eq. (3) to estimate the temperature gradient and gravitational fractionation from the gases isotopes. We use values

of 0.0143 ‰ °C^{-1} for Ω_{15} and for 0.0386 ‰ °C^{-1} for Ω_{40} at 230.5 K or −43.7 °C (Grachev and Severinghaus, 2003). The

385 diffusive column height is calculated from gravitational fractionation using the following equation (simplified from Sowers

et al., 1992):

$$z_{diffusive} = \frac{R \cdot T}{g} \cdot \delta_{grav} \tag{4}$$

where R is the gas constant, T is the temperature, and g is the gravitational acceleration. We used a constant temperature of

229.5 K (−43.7°C), derived from the borehole temperature measurement at 20 m depth in the ABN firn, where season

390 variations do not reach. The average uncertainty for the δ_{grav} is 0.008 ‰, resulting in a 1.5 m uncertainty in the diffusive column

height ($z_{diffusive}$). Pooled standard deviation of $^{15}N_{excess}$ in the ice samples give an analytical uncertainty of 0.0027 ‰, resulting

in a ΔT uncertainty of 0.3°C. Sample preparation includes release of gases in empty lines, and can induce a pressure gradient

leading to small fractionation in both $\delta^{15}N$ and $\delta^{40}Ar$, which is apparently mass-dependant (Severinghaus and Battle, 2006).

In the definition of $^{15}N_{excess}$, mass-dependent processes are cancelled out, and therefore the difference in $^{15}N_{excess}$ between the

395 two samples is smaller than $\delta^{15}N$ or $\delta^{40}Ar$ alone (0.0137 ‰ for $\delta^{40}Ar$ and 0.0036 ‰ for $\delta^{15}N$).

The temperature difference (ΔT) reconstructed from gases is representative of the gradient between the surface and the lock-

in depth. The lock-in depth can be deeper than the diffusive column height in case of near-surface convective mixing.

Therefore, we also estimate the lock-in depth with the gas-ice depth difference at the same age, from the age models (Sect.

2.3, Fig. 4). The gas-ice depth difference decreases over time because of the compaction in the firn and ice column, so we

400 deconvolve the depth difference using a mass-conservative compaction model fitted to the modern profile of snow and ice

density measured in the ABN1314 ice core:

$$\int_{z_{lid}}^{z_{surface}} \rho(z)dz = constant = \int_{z_{gas}}^{z_{ice}} \rho(z)dz \qquad (5)$$

In short, we compute the mass of ice between the depth of gases and ice of the same age, and find the modern depth where the overlying total ice mass up to the surface is identical. In this model, we assume that the density profile remains the same over

405 time. This estimation of the past lock-in depth is called the deconvoluted $\Delta depth_{ice-gas}$. Given the ~20 years uncertainty on the age difference, the deconvoluted $\Delta depth_{ice-gas}$ has an uncertainty of ± 3.8 m.
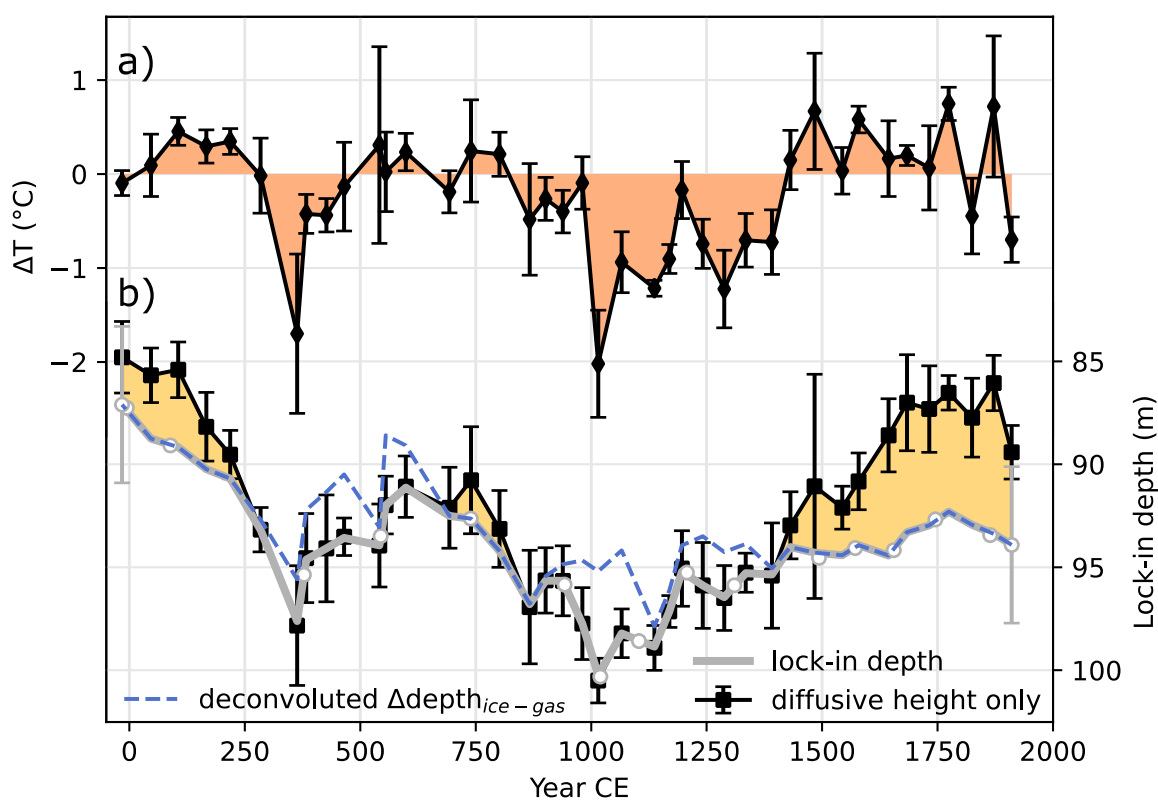
Figure 7. (a) Series of ΔT computed from $^{15}N_{excess}$. Orange shadings indicate a warming ($\Delta T>0$) and blue shadings a cooling ($\Delta T<0$).
410 (b) Past lock-in depth (thick grey line) estimated from diffusive column height of gases isotopes (black line with error bars) and gas-ice depth difference (blue dashed line). Yellow shadings highlight the potential presence of a convection zone that would be located in the uppermost layer of the firn (0~5 m depth), when the lock-in depth appears to be deeper than the diffusive column height. For clarity, uncertainties on the lock-in depth are only shown at both ends of the record. White dots on the lock-in depth indicate the ages where the gas age model was tied to WD2014, indicating the constraints on the $\Delta depth$.

415 Evolutions of the ΔT, deconvoluted $\Delta depth_{ice-gas}$ and diffusive column height are shown in Fig. 7. We define the true lock-in depth (Fig. 7b) as the deepest of diffusive column height and deconvoluted $\Delta depth_{ice-gas}$ because the lock-in depth can be deeper

than diffusive column height in presence of a convective zone, but the lock-in depth should be at least as deep as the diffusive column height. The points where deconvoluted $\Delta depth_{ice-gas}$ (dashed line) is shallower than the diffusive column height are within the 3.8 m uncertainty. They may result from errors in the age model, or in the compaction model: a less-dense than

420 modern profile would yield greater ice-gas depth differences in better agreement with the diffusive column height. However, improved precision is not required in this study, as errors of ± 3.8 m in the lock-in depth result in ± 0.03°C in the surface to lock-in depth temperature gradient, ten times smaller than the uncertainties on the ΔT estimated from the gases isotopes. Changes in the firn depth (lock-in depth) are most likely driven by changes in accumulation, which is itself strongly dependant on ice flow and changes in the local slope (Akers et al., 2022; Fig. A3). The main forcing for the lock-in depth is thus not a

425 temperature factor, we will simply use the value to compute the temperature gradient in the ice sheet (ΔT between surface and lock-in depth).

### 3.2.2 Firn temperature diffusion modelling and inversion

We use an ice advection and densification model with temperature diffusion in the ice column to simulate the evolution of the firn under different temperature scenarios. This model has been previously described in (Orsi et al., 2012) and we use the

430 parameters described in the Appendix A4. Briefly, this model uses a prescribed series of surface temperature, snow accumulation, and bottom geothermal flux to simulate the evolution of temperature in the firn and ice column. In our simulations, densification follows the modern density measurements, and the lock-in depth is inferred from the depth determined previously with deconvoluted $\Delta depth_{ice-gas}$ and diffusive column height. We create 220 temperature simulations by adding a small perturbation ramping up to +1°C on 10 years to a base temperature history estimated from Dome C (Jouzel et

435 al., 2007) and ice-flow related temperature changes (Mouginot et al., 2019, details of the temperature forcings in Fig. A14 and Appendix A4).

We find the optimized temperature history that fits both the present-day borehole temperature profile and the past ΔT temperature gradients estimated from the $^{15}N_{excess}$. The optimized temperature history is estimated by least square regression of a linear combination of the 220 temperature simulations to the borehole temperature profile (e.g., Orsi et al., 2012) and the

440 temperature gradients estimated with $^{15}N_{excess}$ (e.g., Orsi et al., 2014). In this study, we use both borehole and gas data to constrain the temperature history; the borehole temperature profile constrains the long-term changes while the $^{15}N_{excess}$ constrains temperature changes at the scale of ~20 to ~200 years (the diffusion time in the firn column of gases and temperature, respectively). However, the two datasets result in a mismatch on the long-term trends, with $^{15}N_{excess}$ suggesting a cooling trend. To reconcile the $^{15}N_{excess}$ with the borehole temperature profile, a correction of + 0.0046 ‰ is applied on $^{15}N_{excess}$: this

445 minimizes the standard deviation of the temperature reconstruction as it tries to squeeze in rapid temperature changes to arrange for diverging datasets if $^{15}N_{excess}$ is left uncorrected (Figs. A16 and A17). We hypothesize that this $^{15}N_{excess}$ correction for ice samples could be related to expulsion of gases through ice matrix during bubble formation in the firn to ice transition (Severinghaus and Battle, 2006), although the effect on $^{15}N_{excess}$ has never been clearly quantified. We apply the same

correction on all points because it results from physical processes during the formation of bubbles, and we consider it to remain

450 constant at the timescales studied here. A similar correction of + 0.0037 ‰ has been used at WAIS Divide (Orsi, 2013), based
on the mismatch between firn air and shallow ice measurements. This correction implies that the long-term trend is constrained
by borehole temperature rather than $^{15}N_{excess}$ absolute values. Further work in the firn to ice transition is needed to better
quantify the effect of bubble formation on gases isotopic composition.

Ice flow is expected to affect the temperature profile in the ice at ABN, because it advects ice from a location further upstream

455 that was colder when the snow deposited. This can explain the presence of cold ice at depth under ABN, which could be
misinterpreted by the inversion as a climatic warming trend. To account for this effect, we consider the ice in the diffusion-
advection model in a Lagrangian perspective and dissociate temperature changes caused by site displacement and climatic
temperature changes (details and justifications are given in Appendix A4). After inversion of the model, the ice-flow related
temperature changes is subtracted in order to retrieve the climatic temperature changes (Fig. 8). This relies on the assumption

460 that ice flow is in a steady state and the spatial temperature gradient remained constant over the past 2000 years during which
we present our temperature reconstruction.
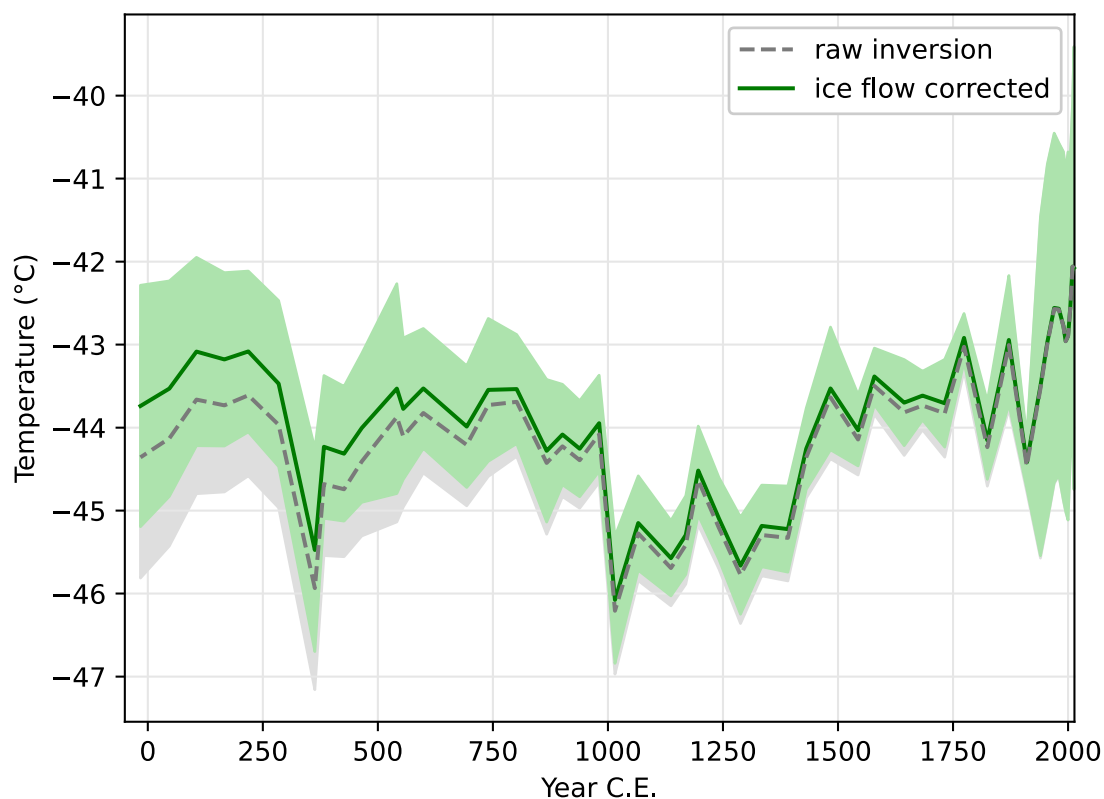
Figure 8. Temperature history reconstructed from the $^{15}N_{excess}$ and borehole temperature inversion. Black dashed line shows the raw measurement and green line shows the glaciology-corrected values. The shading represents errors estimated from the inversion, which depend on measurement precision.

Uncertainties of the diffusion model inversion are calculated following the method described by Orsi et al. (2014), where uncertainty of model parameters are scaled to the uncertainty on ΔT and borehole temperature data used for the inversion. A smoothing parameter is used to constrain the inversion, by limiting the degree of variability of two temperature simulations with perturbation occurring close together in the linear combination used for the inversion. We set the inversion to use an exponentially decreasing covariance in the linear combination, which reaches 0.5 for a time difference of 70 year, roughly twice the time resolution of the gas constraints on ΔT. Finally, a signal to noise ratio parameter is adjusted to force the inversion temperature to fit to the real borehole and ΔT data points within the error, with a minimum cost on the inversion uncertainty (Figs. A18 and A19). The average uncertainty on the temperature reconstruction is $\pm$ 0.7°C.

Climate
of the Past
Discussions

Open Access

EGU

475   **4. Discussion**

4.1 Differences between the reconstructions

The temperature at the ABN ice core site is reconstructed from water stable isotopes (hereafter called $\delta^{18}O$ temperature), and from the inversion of the temperature profile in the borehole and past temperature gradients estimated from inert gas stable isotopes (hereafter called $^{15}N_{excess}$ temperature, Fig. 9). The $\delta^{18}O$ temperature is relatively constant, supporting stable conditions

480   of about –42°C, with less than 1°C change during the past 2700 years, whereas the $^{15}N_{excess}$ temperature is marked by changes of temperature of an amplitude of 2 to 3°C, with cold periods from 300 to 450 CE and from 1000 to 1400 CE, and a recent warming of about 1°C. Although the temperature reconstructions use measurements from the same core, the material used for the reconstructions differ fundamentally, which can explain some of the disparity.

Climate
of the Past
Discussions
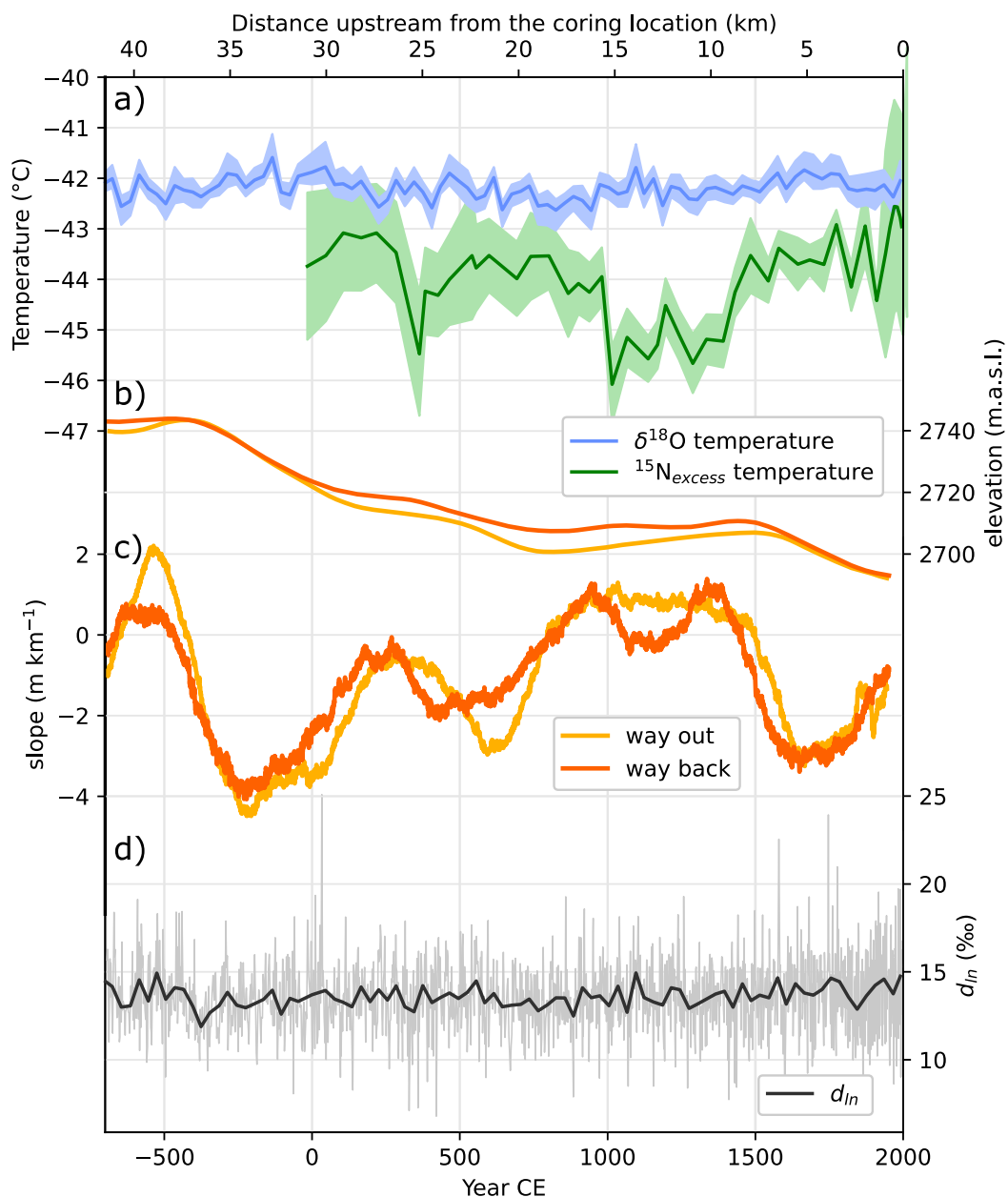
Figure 9. Comparison of (a) δ^{18}O temperature and ^{15}N$_{excess}$ temperature reconstructions with (b) upstream elevation and (c) upstream slopes and (d) d_{ln} in the ABN1314 ice core. Distance upstream is indicated on the top axis, and time is indicated on the bottom axis, the correspondence is relying on the assumption that the ice flowed at a constant rate of 15.4 m yr^{-1} (41.5 km in 2700 years). Error shades in (a) are the error depending on slop used for the reconstruction from δ^{18}O, and the same as in Fig. 8 for ^{15}N$_{excess}$.

First, regarding the time significance, water isotopes in ice are accumulated intermittently during precipitation events, while gases are continuously available, and the temperature permanently diffuses in the ice. The sporadic nature of precipitation and

the consistent warm anomaly associated with precipitation at ABN may cause water isotopes to inaccurately represent the mean temperature (Servettaz et al., 2020). In particular, the cold and dry conditions that can occur on the East Antarctic Plateau

495 are likely to be under-represented in the water isotopes, because a large part of the snow accumulation can be attributed to a few precipitation events (Turner et al., 2019). This may cause the $\delta^{18}O$ temperature to misrepresent the on-average colder periods if they are still interrupted by less-frequent but similarly warm precipitation events, or if the seasonality of precipitation changes with a relatively increased contribution in summer during these cold periods. Additionally, long periods without snow precipitation contribute to increase the snow $\delta^{18}O$ by preferential sublimation of light isotopes (Hughes 2021), smoothing out

500 the signature of cold periods. Here, the precipitation events continue to carry the water isotopes with a constant signature of −42°C. On the other hand, due to the slow diffusion of gases in the firn, the signal integrates temperature variation over a time window of a few decades (Witrant et al., 2012; discussed in Appendix A5), but effectively records the temperature even if there are changes in the accumulation regime. Therefore, changes in the seasonality of precipitations with a shift to drier winters could explain both colder conditions in the winter and a lack of snow accumulation, resulting in the failure of water

505 isotopes to capture the cold conditions in the record (Servettaz et al., 2020).

Second, there is a spatial discrepancy between the two reconstructions: the $\delta^{18}O$ temperature signal is initially acquired in the atmosphere, during the condensation of the precipitation when condensate phase is exchanging with water vapour (Jouzel and Merlivat, 1984), even if it can be modified later (Münch et al., 2017; Casado et al., 2018). The ice temperature is constrained by the snow surface temperature, and the gases in the firn are at equilibrium with the surrounding ice, which temperature thus

510 controls the gases thermal fractionation. Consequently, temperature changes in the snow could be exacerbated by changes in the inversion layer conditions: a more stable inversion layer causes the snow surface temperature to cool much more than the 2 m temperature that was used to calibrate the $\delta^{18}O$ – temperature slope. If changes in the temperature inversion were caused by atmospheric temperature changes, we would still expect the $\delta^{18}O$-derived temperature reconstruction to reflect the changes observed in the gas-based temperature reconstruction, albeit with a weaker amplitude. This has been the case for example for

515 glacial – interglacial transition in West Antarctica: the snow temperature has varied with greater amplitude than what the water isotopes have recorded (Buizert et al., 2021). However, here, the cold periods identified with the gas and borehole temperature reconstruction are not matched by any sign of cooling in the $\delta^{18}O$ record, suggesting that the differences are not entirely caused by atmospheric temperature changes amplified by the temperature inversion.

Another possible origin for the difference between atmospheric and surface snow temperatures is that surface winds weaken

520 the inversion by causing turbulent mixing of the stratified air layers near the surface (Hudson and Brandt, 2005; Pietroni et al., 2014). Given that the average katabatic wind speed increases with the terrain slope (Parish and Waight, 1987; Parish and Bromwich, 1991; Vihma et al., 2011), we investigated possible effects of elevation and topographic slope changes on the recorded temperature (Fig. 9). Although it was taken along the ice stream flowline and not the katabatic wind flowline, the terrain elevation and slope roughly provides information of what slope-induced changes in katabatic winds may have affected

525 the ABN site as it drifted (Fig. 9b and 9c). It appears that ABN site was on a plateau with a null slope between 18 and 8 km

upstream from the coring location, which roughly corresponds to the 800 to 1500 CE period, slightly longer than the cold period identified with $^{15}N_{excess}$ temperature (Fig. 9a). It is possible that a reduction of katabatic winds on this part of the terrain allowed for a stronger near-surface temperature inversion to settle, effectively cooling the snow relative to the atmosphere. Nevertheless, the recent warming of 1°C cannot be attributed to changes in the slope as the warming is occurring while the

530 slope gets gentler.

Influence of temperature on $\delta^{18}O$ could be masked by a concurrent change in moisture source: e.g., if cold periods were associated with a shift towards warmer source, the two effects could compensate each other and result in a constant $\delta^{18}O$. Such a change in moisture source can be recorded in the d_{ln}, which efficiently tracks changes in the moisture source temperature (Uemura et al., 2012; Markle and Steig, 2022). The d_{ln} series shows no significant trend, with the values averaging 13.6 ‰.

535 When averaged on 30-years to smooth out noise, the standard deviation of d_{ln} is only 0.6 ‰, with no remarkable change during the cold periods in the $^{15}N_{excess}$ temperature. This suggests that there was minimal to no change of the moisture source affecting the variability of $\delta^{18}O$, and thus confirms that the condensation temperature remained relatively stable for the last 2700 years. In a recent study, Morgan et al. (2022) suggest that the gas stable isotopes in the firn could be affected by seasonal rectification: in absence of mixing of air in the surface layer, the winter temperature inversion cools the snow surface and densifies the near-

540 surface firn air which could sink and advect the air column downward more efficiently than during summer. Winter advection of air down into the firn lowers the $^{15}N_{excess}$ isotopic signal, which can result in an apparent colder ΔT. Sinking air is suspected to occur when katabatic wind and surface turbulence are weak, which allow a strong temperature inversion to develop. On the other hand, strong katabatic winds induce a mixing of both the air above the snow surface where temperature inversion is the strongest, and the air in the uppermost layer of the firn, increasing the convection layer. Morgan et al. (2022) hypothesize that

545 the change in surface slope and curvature, which affect the strength of katabatic winds (Vihma et al., 2011), may in turn be responsible for some difference in the ΔT derived in the isotopes, along with snow accumulation and the lock-in depth. Surface topography changes are linked to the glacial flow both at South Pole (Morgan et al., 2022) and ABN, two Antarctic sites that are not on an ice divide.

At ABN, the periods with suspected upper firn convection (yellow shadings, Fig. 7b) correspond to periods with positive ΔT

550 (orange shading, Fig. 7a), whereas periods with deepest lock-in depths are associated with very negative ΔT. The existence of a convective zone may be linked to the surface wind speed, as ABN was in the steeper part of the slope during the periods with a convective zone (Fig. 9b). However, the late Holocene conditions are unlikely to result in a strong rectifier effect at ABN, because this site is located on a slope where there is expected sustained surface winds, and even at South Pole where temperature is on average 7°C colder than ABN does not support a rectifier effect on the Holocene (Morgan et al., 2022).

555 Although the ΔT – lock-in depth correlation may be linked to past variations of winds caused by topographic slope, low temperatures resulting from climate variability may also be responsible for an increased lock-in depth due to slower densification (Goujon et al., 2003). Rather than a firn rectifier effect, the ABN temperature reconstruction may be simply

reflecting changes in the snow temperature mirroring near-surface temperature inversion strength, influenced by average wind speed and local slope.

560   To summarize, there is possibility that water isotopes are biased towards warm temperatures because of lack of precipitation in cold periods, and that gas isotopes reflect topography-driven changes in wind speed and temperature inversion strength. We expect the temperature history to be in between the two estimations, although the $^{15}N_{excess}$ should more consistently record temperature changes at the snow surface.

4.2 History of temperature across the East Antarctic Plateau

565   Many regions of the globe including Antarctica have been marked by a cooling trend during the past 2000 years, until the beginning of the industrial era (PAGES 2k Consortium, 2013). Climate history of the Antarctic region was reconstructed from ice core water isotopes (Stenni et al., 2017), with some cores on the East Antarctic Plateau where ABN is located (EDC, TALDICE), and the coastal region of Wilkes land (Law Dome, location of coring sites is indicated on Fig. 1). We selected ice cores from the Antarctica2k database (Stenni et al., 2017) that cover at least the past millennium until the pre-industrial era

570   (1000–1900 CE) and plotted the $\delta^{18}O$ or δD, representative of the temperature, and their 1000 to 1900 CE trend for each core (Fig 10). To avoid biases based on differing calibration methods, comparisons are made using isotope values directly (δD or $\delta^{18}O$). For comparison, each core was resampled at a 30-year resolution, and the trends were computed on the 900 years spanning from 1000 to 1900 CE (31 points); trends are significant if $r^2 \geq 0.13$ (p-value < 0.05). While Stenni et al. (2017) report a general cooling trend both for Wilkes coast and East Antarctic Plateau on the past 2000 years, we find that the last

575   millennium is not marked by any significant trend in the plateau ice cores, when taken separately. On the other hand, the coastal ice core from Law Dome shows a slight cooling trend (decreasing $\delta^{18}O$). The $\delta^{18}O$ record from the ABN1314 ice core has a higher temporal resolution than other East Antarctic Plateau ice cores, but its absence of a significant trend supports the previous findings pointing to stable atmospheric conditions during the past 2000 years on the East Antarctic Plateau. However, the $\delta^{18}O$ records on the east Antarctic Plateau are subject to debate whether they can effectively reflect rapid temperature

580   changes, due to low accumulation rates and intermittent accumulation events (Münch et al., 2017; Casado et al., 2020). In any case, the $^{15}N_{excess}$ temperature variability strongly contrasts with $\delta^{18}O$ records from ABN1314 and other East Antarctic Plateau ice cores.

585
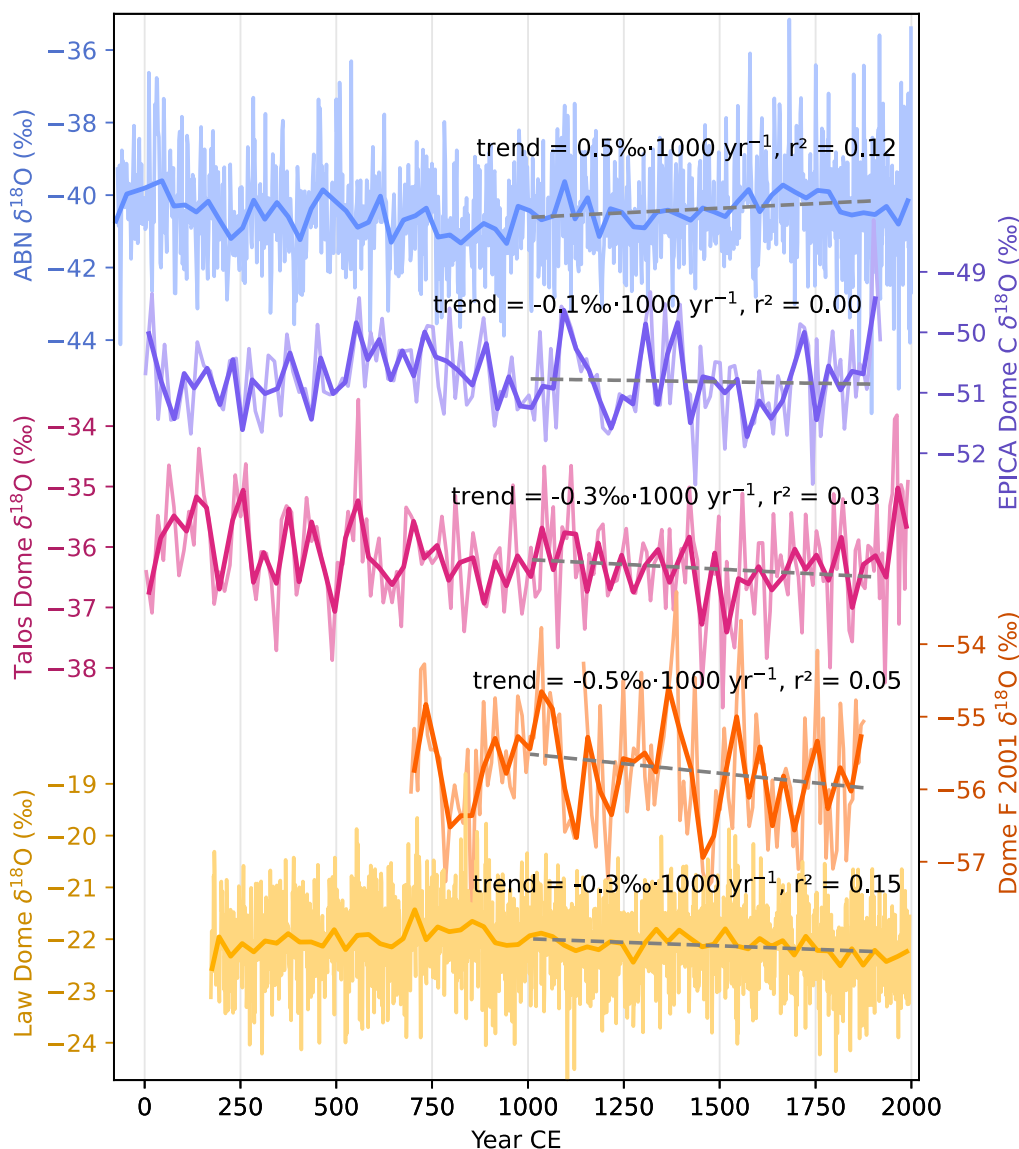
Figure 10. Comparison of δ^{18}O records from ABN1314 core and a selection of nearby ice cores from the Antarctica2k database (Stenni et al., 2017). Thin lines: full resolution, thick lines: resampled at 30-year resolution. Trends are computed from the 30-year 590 resampled series, and are significant if r²>0.13 (p-value < 0.05, n = 31)

In particular, in the $^{15}N_{excess}$ and borehole-based reconstruction (Fig. 11a), the temperature at ABN varies between –44.5°C and –43°C after 1750 CE but stabilizes at an average of –42.5°C after 1975 CE. After 1900 CE, the temperature inversion is mainly constrained by the borehole temperature, and this warmer phase can be seen in the steepening gradient of the temperature above 100 m below surface (Fig. 3). This temperature of –42.5°C is about 1°C warmer than the 1500–1850 CE 595 average and could reveal the effect of recent warming in East Antarctica. This surface warming at ABN is unlikely to be caused

Climate
of the Past
Discussions

by a topographic change as the slope is flattening near the drilling site (Fig. 9) and would on the contrary favour the slowing of katabatic winds and surface cooling by strengthening of the near-surface temperature inversion. The absence of further warming on the East Antarctic Plateau after 1975 is consistent with observations and could be related to the compensation effect associated with the positive trend in the southern annular mode in the later part of the 20th century (Nicolas and

600 Bromwich, 2014; Fogt and Marshall, 2020). A similar warming of about 1°C inferred from East Antarctic borehole temperatures has been reported in locations near the ice divide of Dronning Maud Land, but was equivocal, as a borehole off the divide showed a possible cooling trend except for the most recent couple of years (Muto et al., 2011). The $^{15}N_{excess}$ and borehole temperature reconstruction provides new insight on the climate of East Antarctica that may complement the many $\delta^{18}O$ records in this region. Three independent sources of data support this varying temperature history: the borehole

605 temperature, the gas $^{15}N_{excess}$ and the lock-in depth. Together they consolidate the evidence that surface temperature changed with a greater amplitude than what $\delta^{18}O$ suggests.

4.3 Atmospheric teleconnections

In Antarctica and the Southern Hemisphere, the main mode of atmospheric variability is the Southern Annular Mode (SAM), with a strong signature on Antarctic temperature (Marshall and Thompson, 2016). The SAM describes the surface pressure

610 difference between mid and high latitudes (Marshall, 2003; Fogt et al., 2009), and a positive phase denotes a strong pressure gradient. On the East Antarctic Plateau, SAM phase and surface temperature are anti-correlated because a positive SAM phase is associated with a reduced meridional heat transport (Marshall and Thompson, 2016), and the SAM signature is found in the temperature at the ABN site, although its effect on $\delta^{18}O$ is less prominent (Servettaz et al., 2020). The variability of SAM is linked to other climate modes and parameters such as El Niño – Southern Oscillation (Abram et al., 2014), Atlantic Meridional

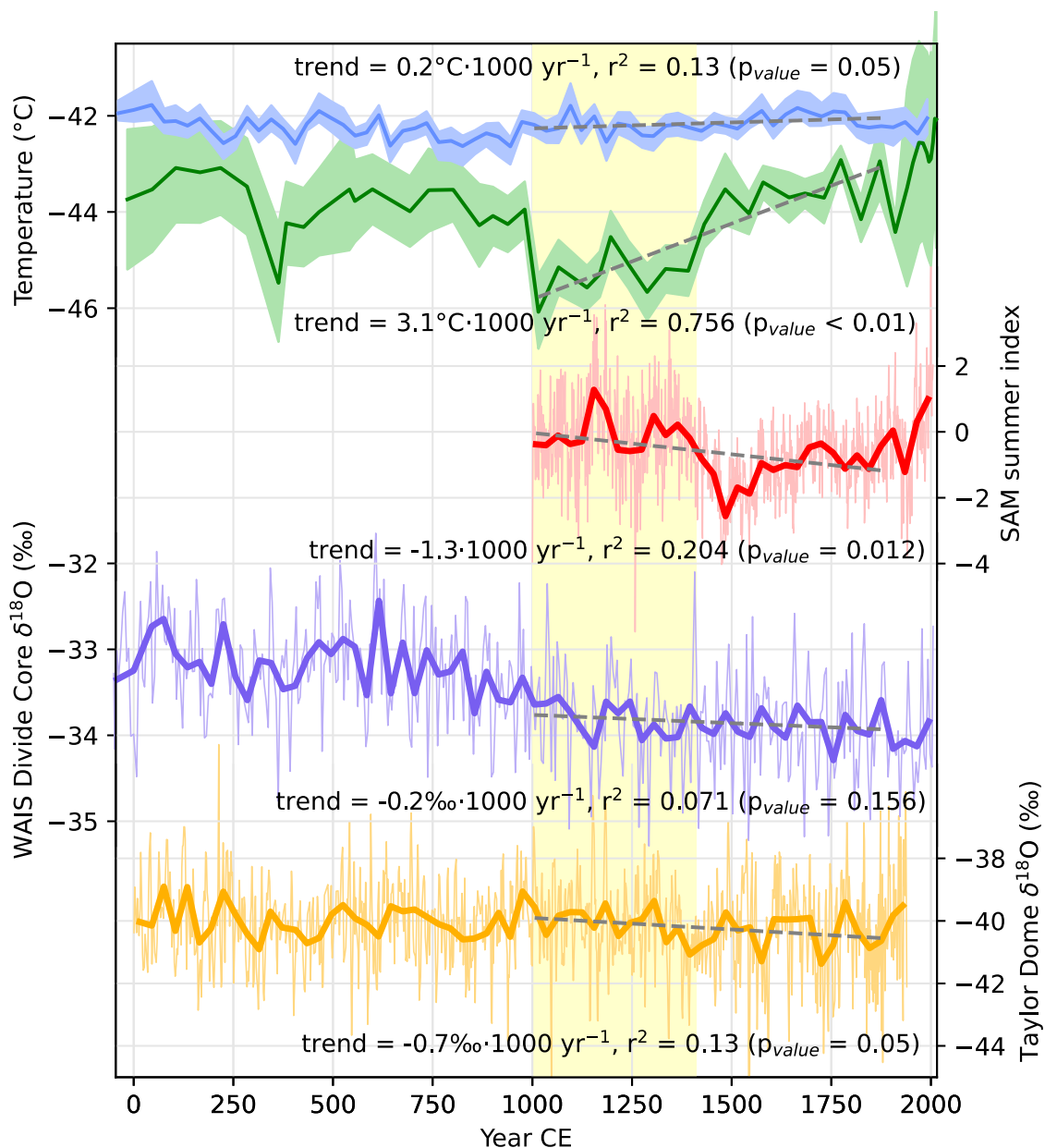615 Overturning Circulation (Pedro et al., 2018) and solar irradiance (Wright et al., 2022).

Figure 11. (a) δ^{18}O temperature and ^{15}N$_{excess}$ temperature reconstructions (this study). Error shades are the same as in Fig. 9. (b) Southern Annual Mode (SAM) annual reconstruction (Dätwyler et al., 2018). Thin lines show the annual reconstruction. (c) West Antarctic Ice Sheet (WAIS) Divide ice core δ^{18}O (Steig et al., 2013). Thin lines show the 5-year average. (d) Taylor Dome δ^{18}O (Steig et al., 2000). Thin lines show the full resolution. All thick lines in this Figure Ahow the 30-year average, except for ^{15}N$_{excess}$ temperature which has a resolution of about 45 years. Yellow shading highlights the 1000–1400 CE period during which the ^{15}N$_{excess}$ temperature is significantly colder, in phase with a positive SAM index. WAIS Divide and Taylor dome δ^{18}O data were taken from the Antarctica2k database (Stenni et al., 2017), where Taylor dome is on its updated TD2015 timescale (Sigl et al., 2014).

On the time scale of a thousand years, the SAM has been reconstructed from paleoclimate proxies sensitive to SAM-related
625   temperature anomalies (Abram et al., 2014; Dätwyler et al., 2018). The two reconstructions yielded similar trends, although
the reconstruction of Abram et al. (2014) shows more amplitude due to being calibrated on the instrumental period with annual
SAM indices (Wright et al., 2022). Here we will only show the annual SAM reconstruction from (Dätwyler et al., 2018; Fig.
11b), which relies largely on the same proxies, but with a correlation plus stationarity criterion for proxy selection. During the
1000–1400 CE period, the SAM was in a relatively positive phase, followed by a net switch to a strongly negative phase that
630   lasted until about 1800 CE. The $^{15}N_{excess}$ temperature at ABN is remarkably consistent with the SAM variability, as it shows
colder temperatures during the positive phase of the SAM in the beginning of the last millennium, with rapidly increasing
temperature as the SAM changes to the negative phase. Although the SAM reconstructions do not extend beyond 1000 CE,
sea ice proxies in the nearby Adélie Basin (66° S, 140° E) suggest that the positive SAM phase may have started around 830
CE (Crosta et al., 2021), which is sensibly earlier than the $^{15}N_{excess}$ temperature decrease observed at ABN at around 1000 CE.
635   Across Antarctica, the West Antarctic Ice Sheet (WAIS) Divide ice core shows a shift in $\delta^{18}O$ from −33.2 ‰ on the 0–1000 CE
period to −33.8 ‰ on the 1000–1400 CE period (Fig. 11c, Steig et al., 2013). Although less abrupt than the change observed
in $^{15}N_{excess}$ temperature, this shift may reflect a change driven by positive SAM on West Antarctic temperature. Moreover,
particle size distributions in the WAIS Divide ice core suggest that a poleward contraction of Southern Westerly Wind belt
during the 1050–1430 CE period, marking a positive SAM phase (Koffman et al., 2014). Nevertheless, the transition to a
640   negative SAM phase after 1400 CE is not accompanied by a warming in West Antarctica, suggesting that other mechanisms
compensate for the SAM effect on WAIS Divide ice core $\delta^{18}O$.

By the same way SAM is defined as the first Empirical Orthogonal Function (EOF) of geopotential height, the Pacific South
American modes PSA1 and PSA2 are the second and third EOFs of geopotential height, and represent the zonally asymmetric
variability in the Pacific sector of Antarctica (Marshall and Thompson, 2016). Even though its intensity is weaker, the PSA2
645   has a more widespread temperature effect on Antarctic temperatures: a positive PSA2 is associated with warm anomalies in
East Antarctica, while cold anomalies affect West Antarctica and the Eastern Ross Sea (Marshall and Thompson, 2016). The
opposing trends in the $^{15}N_{excess}$ in ABN, East Antarctica (+2.9°C 1000 yr^{-1}, r^2 = 0.76) and $\delta^{18}O$ in WAIS Divide Core in West
Antarctica (−0.2 ‰ 1000 yr^{-1}, r^2 = 0.07) are in line with an increase of the PSA2 phase over the 1000–1900 CE period. An
increase in the PSA2 phase could indeed explain the cooling trend observed in both in WAIS Divide and Taylor Dome
650   (−0.7 ‰ 1000 yr^{-1}, r^2 = 0.13; Fig. 11d, Steig et al., 2000), despite the change to a more negative SAM (−0.7 1000 yr^{-1}, r^2 =
0.19). The low significance of trends in WAIS Divide core $\delta^{18}O$ could result from the compensating effects of a switch to a
more positive PSA2 (cooling effect on WAIS) and a more negative SAM (warming effect on WAIS).

Increased katabatic winds in the Eastern Ross Sea under a transition to a positive phase of PSA2 could support an opening of
the polynya in the East Ross Sea around that time, as suggested by an increase of δD in the Roosevelt Island Ice Core in the
655   Ross Sea (Marshall and Thompson, 2016; Bertler et al., 2018). The decreasing accumulation of both Roosevelt Island and
West Antarctic Ice Sheet during the last millennium (Bertler et al., 2018) is also compatible with a positive trend in the PSA2

(Marshall et al., 2017). Such a change in the PSA2 would have atmospheric and oceanic implications beyond the few records discussed here, and it is still unclear what is the long-term trend of secondary climate modes in Antarctica, such as PSA1 or PSA2. Despite their relatively low contribution to climate variability on instrumental era, it is possible that the long-term

660   variability of PSA modes had a greater amplitude owing to changing atmospheric conditions in the Ross Sea related to the ongoing retreat of the Ross ice shelf during the late stages of the Holocene (Yokoyama et al., 2016). The increasing number of high-resolution paleoclimate records in the Antarctic region may help to investigate the past variability of secondary atmospheric modes, similarly to what has been done for the SAM (Abram et al., 2014; Dätwyler et al., 2018), but this is beyond the scope of this study.

665   **5. Conclusion**

We have reconstructed past temperature variability over the last 2000 years from an ice core drilled at Aurora Basin North (ABN), inland East Antarctica. We used two temperature reconstructions: (1) based on water stable isotopes ($\delta^{18}O$) and (2) by inversion of a diffusion model matching borehole temperature and past temperature gradients recorded in gases stable isotopes ($^{15}N_{excess}$). The ABN drilling site is located far from a divide, so we carefully took the ice flow into account when estimating

670   the past temperature, and we were able discuss the climate variability in East Antarctica at a high resolution on the past 2000 years.

The two temperature reconstructions from the same ice core show major differences, that are attributed to the difference of spatial and temporal significance of the proxies used: the water stable isotopes acquire their signal during condensation in the atmosphere and are accumulated sporadically during snowfall events; whereas the borehole temperature and gases are

675   constantly exchanging with snow surface conditions, and thus integrate the snow surface temperature over a few decades. While the $\delta^{18}O$ temperature reconstruction shows little to no trend over the past 2000 years, consistently with other East Antarctic Plateau ice cores, the $^{15}N_{excess}$ and borehole temperature inversion suggests that surface temperature varied with an amplitude of about 2°C. A cold period during 1000–1400 CE matches a positive phase of the Southern Annular Mode (SAM), known to have a cooling effect on most of Antarctica (Marshall and Thompson, 2016). The surface warming at ABN after

680   1400 CE contrasts with West Antarctic $\delta^{18}O$ records and indicates the influence of zonally asymmetric Pacific-South American atmospheric modes. Prevalent cold and dry winter during cold periods may explain both the inability of water isotopes to record temperature changes, and the lower-than-average surface snow temperature. The $^{15}N_{excess}$ temperature reconstruction seems to better track surface temperature changes than $\delta^{18}O$, albeit with a lower temporal resolution, as shown by its remarkable consistency with SAM variability. This work highlights the importance of using diverse proxies in temperature

685   reconstructions, and motivates further studies to understand the proxies used, beyond simple linear relationships.

Appendix A: Supplementary information on data production

Appendix A1 Age Models
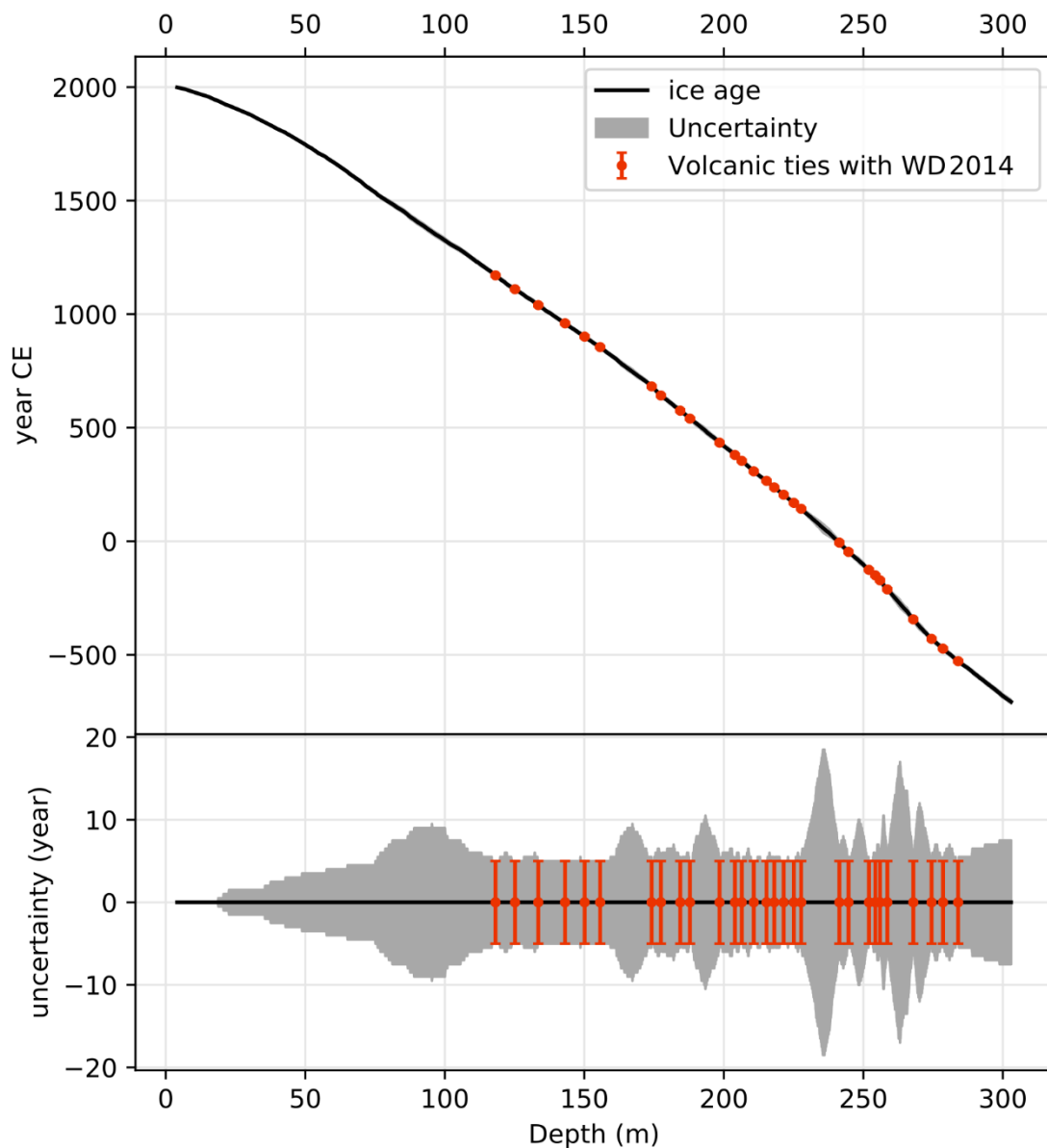

Figure A1. Age model for the ABN1314 core. The grey shading indicates cumulated uncertainties on annual layer counting. Volcanic horizons were identified on the sulphur record and were tied to the ages of volcanic events on WD2014 timescale (Sigl et al., 2015, 2016), and given a 5-year uncertainty, corresponding to the maximum intrinsic uncertainties on WD2014 timescale for this period.
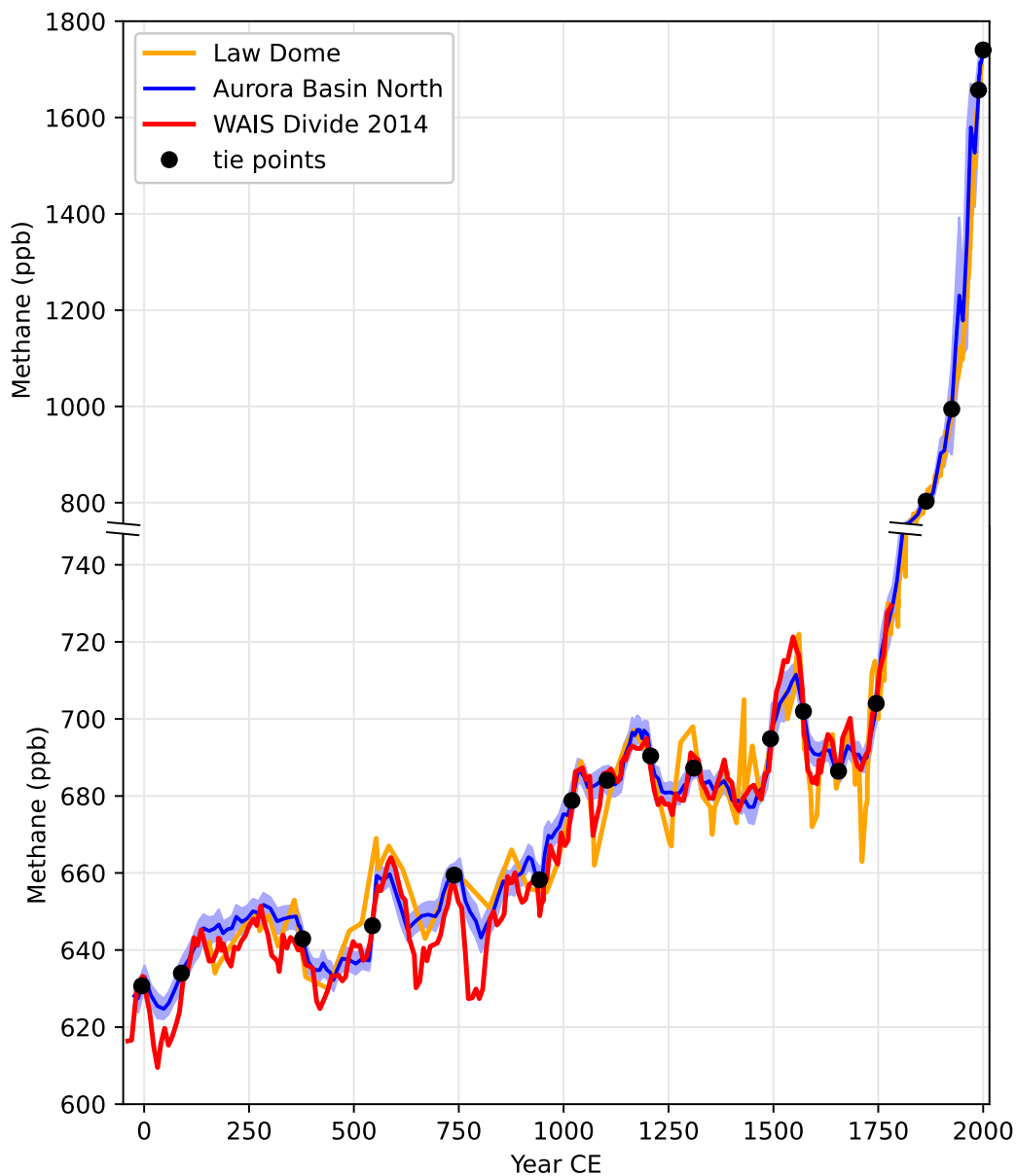
Figure A2. Methane concentration in trapped air in ABN1314 (blue) averaged on 1 m sections (the light blue shading shows the 1σ standard deviation of measurements in the 1 m section, measured on Continuous Flow Analysis system), West Antarctic Ice Sheet (WAIS) Divide (red, Mitchell et al., 2011), and Law Dome (orange, Rubino et al., 2019), on WD2014 gas timescale (Sigl et al., 2015, 2016). Vertical axis changes scale with an axis break at 750 ppb.

695

Climate
of the Past
Discussions

Appendix A2 Ice-flow related changes
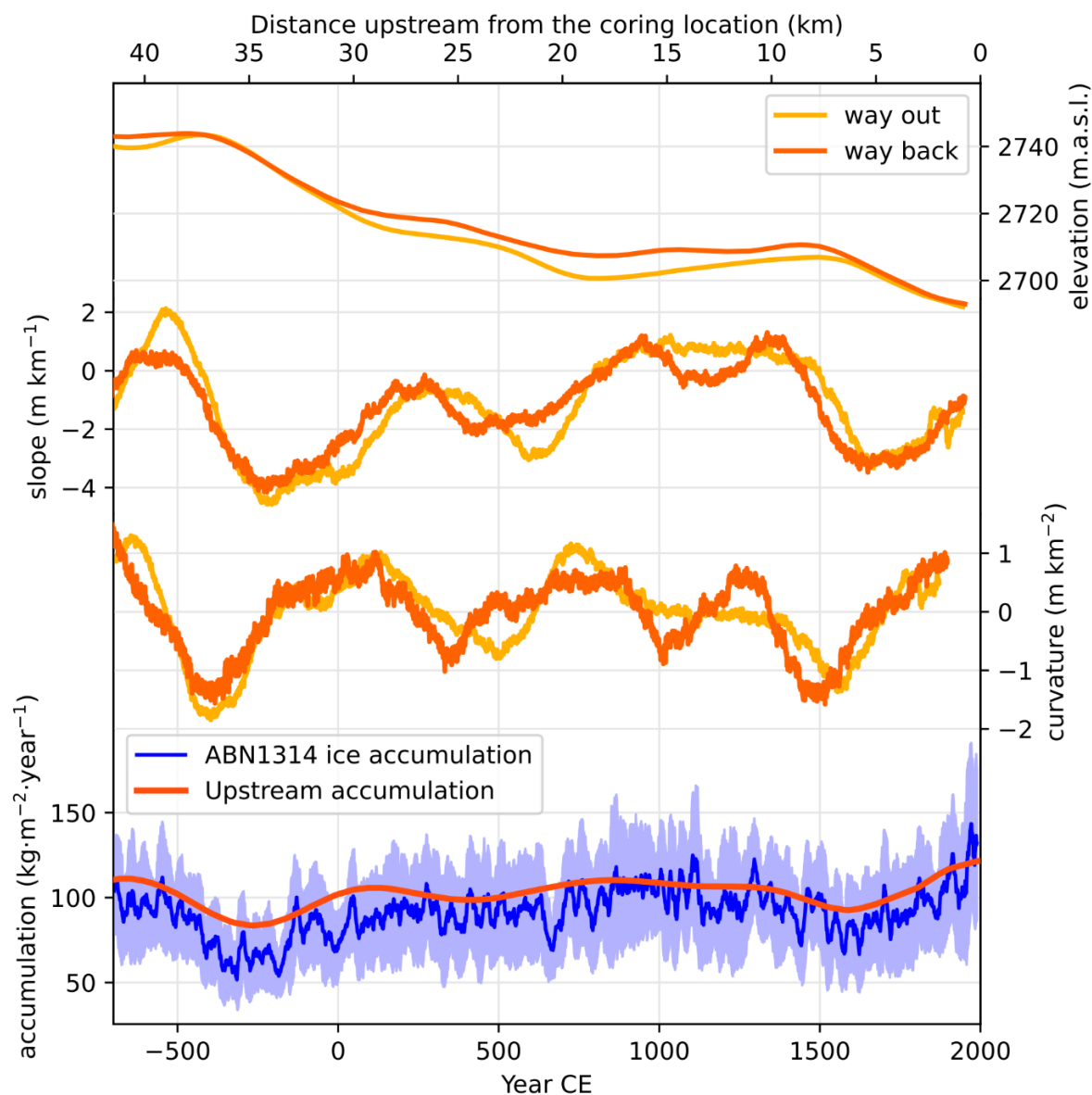
**Figure A3. Upstream elevation, slope, curvature, and accumulation compared to the ice accumulation in the ABN1314 core. ABN
ice accumulation was calculated with the layer thickness from Annual Layer Counting and the density profile measured by weighing
known volumes of the ice core, and is shown with a 20-year running mean to smooth out the reconstruction. The light blue shading
shows the 20-year standard deviation. Upstream accumulation is estimated by integrating the ice mass between surface and first
isochrone reflector in the ground penetrating radar profile. We used the density profile measured in the ABN1314 ice core to estimate
the mass, assuming the density upstream follows a similar profile, and we inferred the age of the isochrone from the age at the
corresponding layer in the ABN1314 ice core. Ice movement since deposition is estimated by varying the spatial length of the upstream
accumulation record sampled to maximise the correlation with the 2700 year temporal accumulation record from the ABN ice core
(lower panel).**
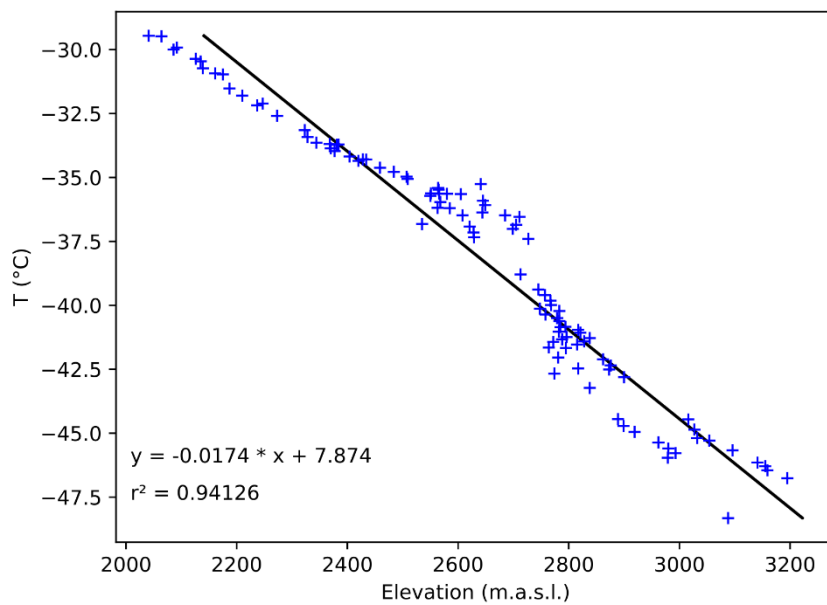
**Figure A4. Temperature – elevation slope in the 2000 – 3250 m.a.s.l. elevation range in East Antarctic traverses with site temperature
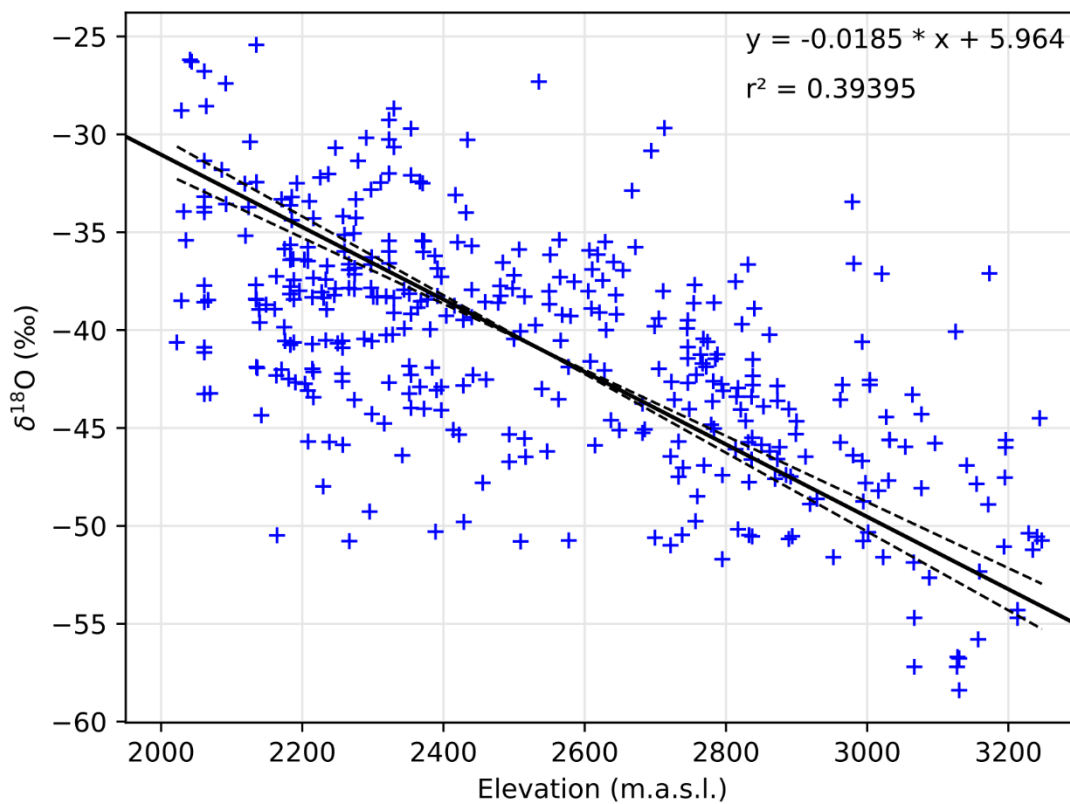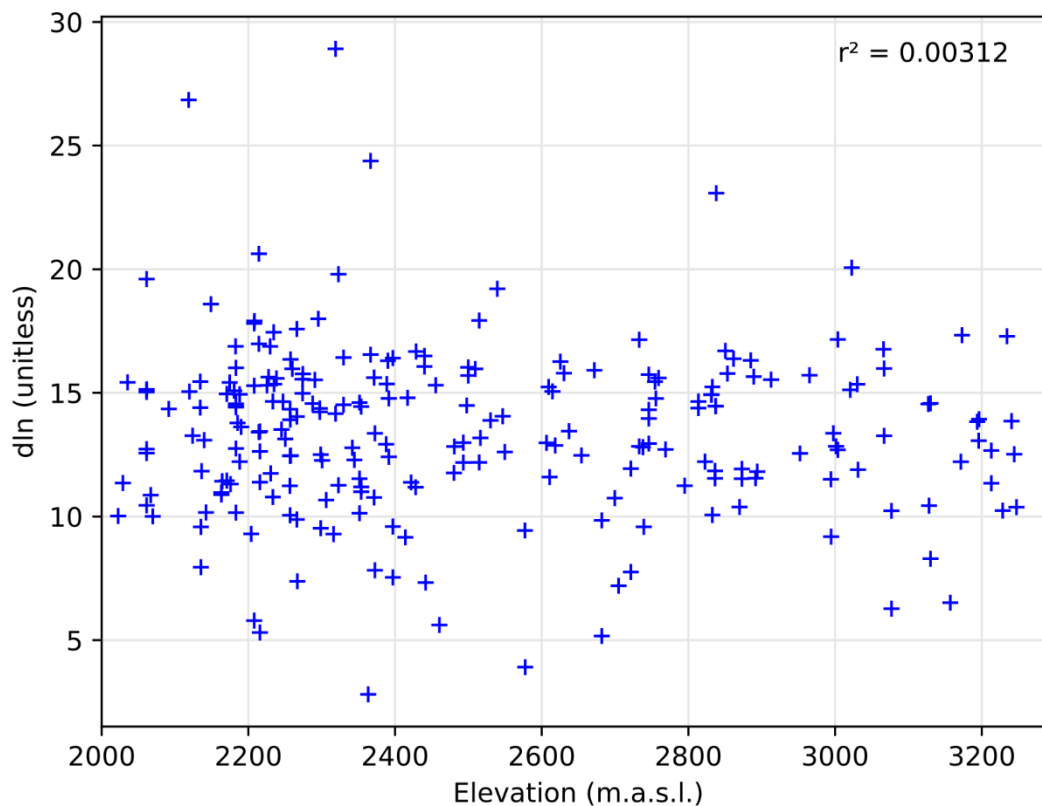estimations (Xiao et al., 2013; Pang et al., 2015).**

Figure A5. δ¹⁸O – elevation slopes in surface snow studies: Zongshan to Dome A traverses (Xiao et al., 2013; Pang et al., 2015) and (Goursaud et al., 2018). We restricted our slope to sites at elevations comprised between 2000 and 3250 m.a.s.l., and longitudes from 80°E to 160°E.

Figure A6. d$_{ln}$ − elevation scatterplot in (Goursaud et al., 2018) database, restricted to sites at elevations comprised between 2000 and 3250 m.a.s.l., and longitudes from 80°E to 160°E.

Appendix A3 Calibration and corrections of isotopic composition of gases

Measurement of gases from ice cores and their correction have been extensively described by Severinghaus et al. (2001). In addition to their corrections of pressure imbalance (section 3.1 of this document) and chemical slope (section 3.2), we introduce a specific correction for focus drift (section 3.3) before the normalization to atmosphere, which is the standard for the gases isotopes measured in this study (section 3.4).

Appendix A3.1 Pressure imbalance correction

In a dual inlet mass spectrometer, two bellows alternatively supply gas to the spectrometer source. Possible differences in the pressure of each bellow can influence the beam intensity and thus measured δ values. This effect quantified using daily-determined Pressure Imbalance Slopes (PIS), where the volume in the bellows is forced into asymmetrical state to evaluate the effect on isotope ratios (for example Fig. A7). The pressure imbalance (ΔP) is defined by the difference of intensity (*int*) between sample and standard of the main gas measured ($^{28}N_2$ in nitrogen configuration or ^{40}Ar in argon configuration).

$$\text{PIS}_{40_{Ar}} = \frac{\Delta\delta^{40}\text{Ar}}{\Delta P} \tag{1}$$

730   Isotopic measurements are then corrected using daily PIS and imbalance during measurement, as shown in Eq. (2).

$$\delta^{40}\text{Ar}_{\text{PI corrected}} = \delta^{40}\text{Ar}_{\text{raw}} - \text{PIS}_{40_{Ar}} \times \Delta P \tag{2}$$

Equivalent slopes and corrections were performed for δ^{15}N. ΔP is calculated with intensities averaged on entire blocks for standards (11 integrations) and samples (10 integrations). Pressure imbalance correction is applied block by block, and the standard deviation of 5 blocks of argon in a sequence typically decreases from 0.020 ‰ to 0.015 ‰ (0.005 ‰ improvement).

735   The pressure imbalance corrected values are compared to raw values in Fig. A8. The Pooled Standard Deviation (PSTD) in Fig. A8 is given for ice replicates, and is therefore larger than the standard deviation of block-averaged δ values within a sequence, for a unique sample.
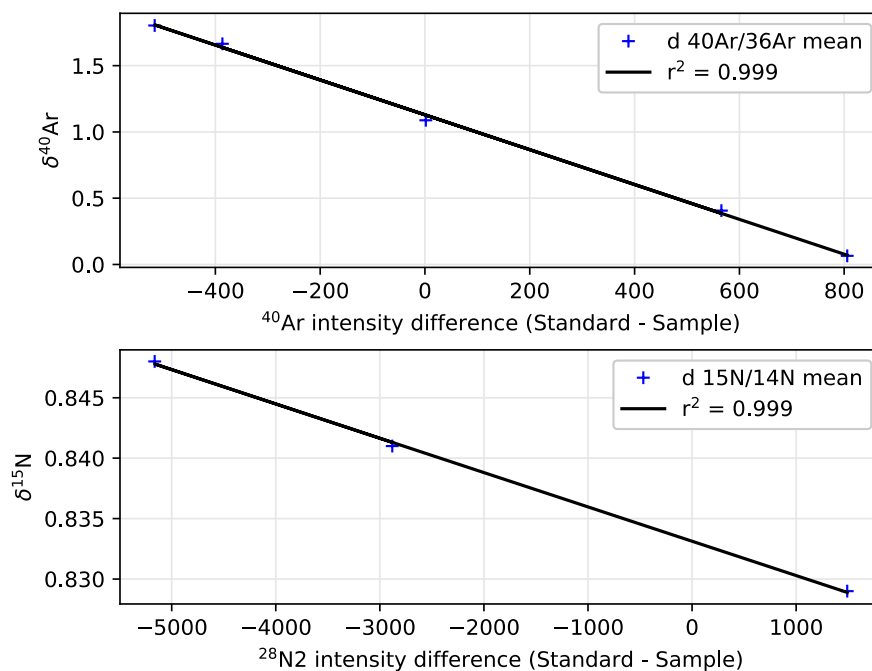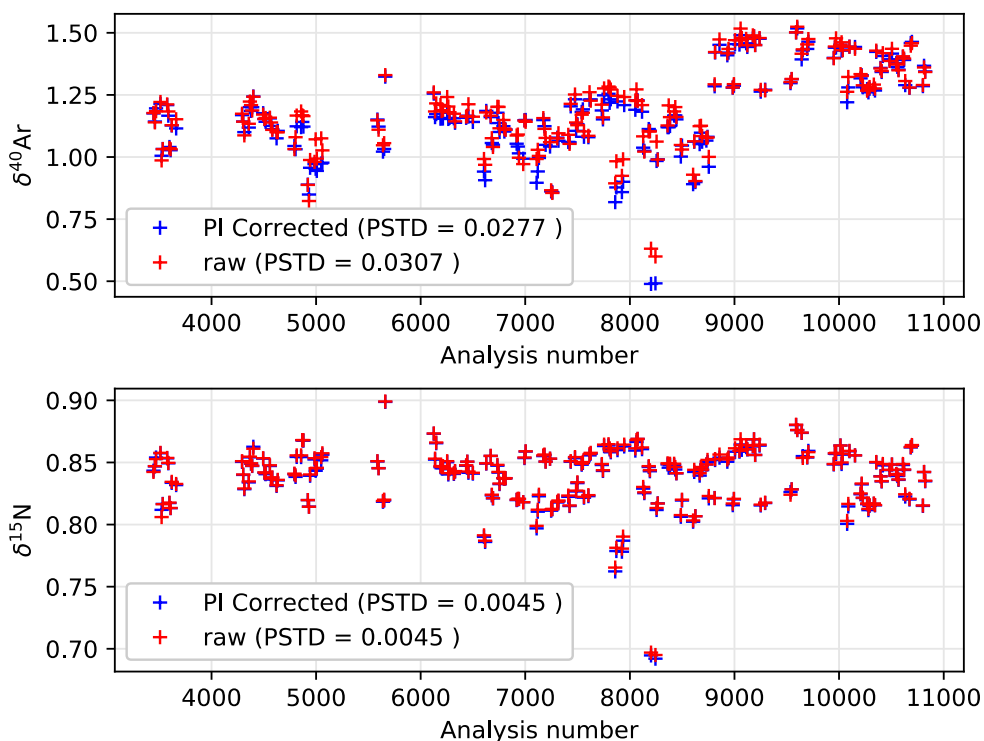

Figure A7. Variability of δ^{40}Ar and δ^{15}N as a function of intensity difference between sample and standard.

Figure A8. Comparison of δ^{40}Ar and δ^{15}N before and after pressure imbalance correction for all the measurements. Analysis number corresponds to the number of blocks proceeded, measurements were performed between February and December of 2019. Pooled Standard Deviation (PSTD) of each series are indicated in the captions.

Appendix A3.2 Chemical Slope correction

745 The gas supplied to the spectrometer and ionized by the filament is a mixture of argon (about 1 %) in nitrogen (about 99 %) with very few other gases. The elemental ratio of argon to nitrogen can modify how effectively the argon will be ionized, because of charge transfer in the source. Therefore, the relative quantity of argon in the mixture can affect the δ^{40}Ar measured by the spectrometer. The chemical ratio effect is quantified by preparing collector tubes of pure nitrogen with varying amount of standard argon of known isotopic composition. We determine the ratio of Ar/N_2 with peak jumping, and measure the δ^{40}Ar

750 over 5 blocks for each mixture. The slope is defined in Eq. 4, and illustrated by Fig. A9.

$$\text{CS}_{^{40}\text{Ar}} = \frac{\Delta\delta^{40}\text{Ar}_{\text{PI corrected}}}{\Delta\delta\text{Ar}/N_2} \tag{3}$$

We apply the chemical slope correction on the δ^{40}Ar values averaged on a full sequence, because the elemental mixture does not change within a sample.

$$\delta^{40}\text{Ar}_{\text{CS corrected}} = \delta^{40}\text{Ar}_{\text{PI corrected}} - \text{CS}_{^{40}\text{Ar}} \times \delta\text{Ar}/N_2 \tag{4}$$

755 The chemical slope was measured after each change in the filament and if the filament was put in contact with air, as it may cause change in the ionization rate and therefore the chemical slope. Consequently, we only have three chemical slope

38

measurements for 8 months: at the beginning, in the middle and at the end. This correction does not result in an immediate improvement of the Pooled Standard Deviation (Fig. A10), because the chemical slope error is partly compensated by a drift error (next section), so correcting only the first effect induces a small increase in the sample difference.
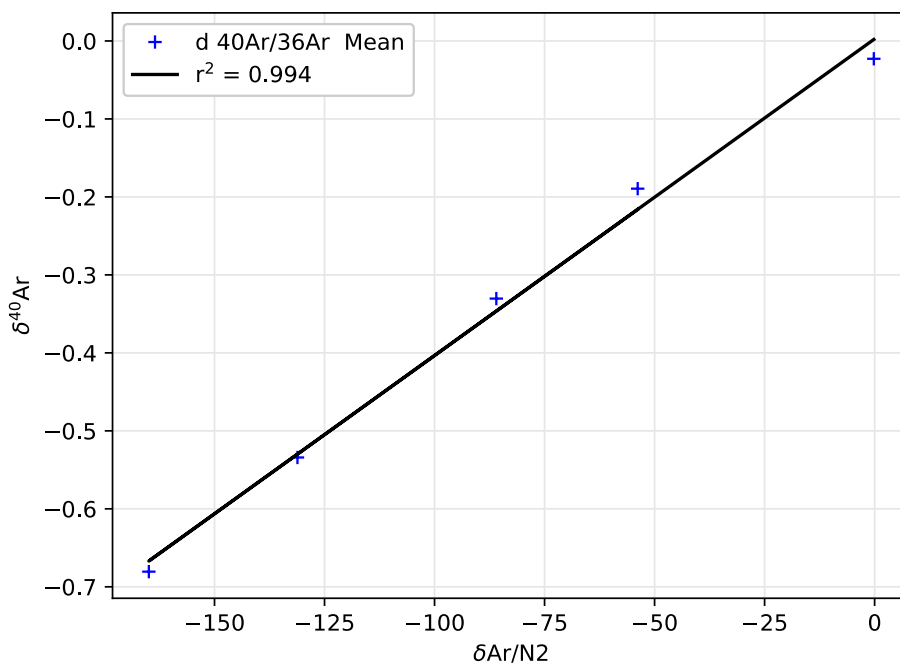
760

Figure A9. Chemical Slope: variability of δ^{40}Ar versus δAr/N$_2$. Larger concentration of Ar in the gas mixture introduced into the spectrometer tend to increase the δ^{40}Ar values measured.
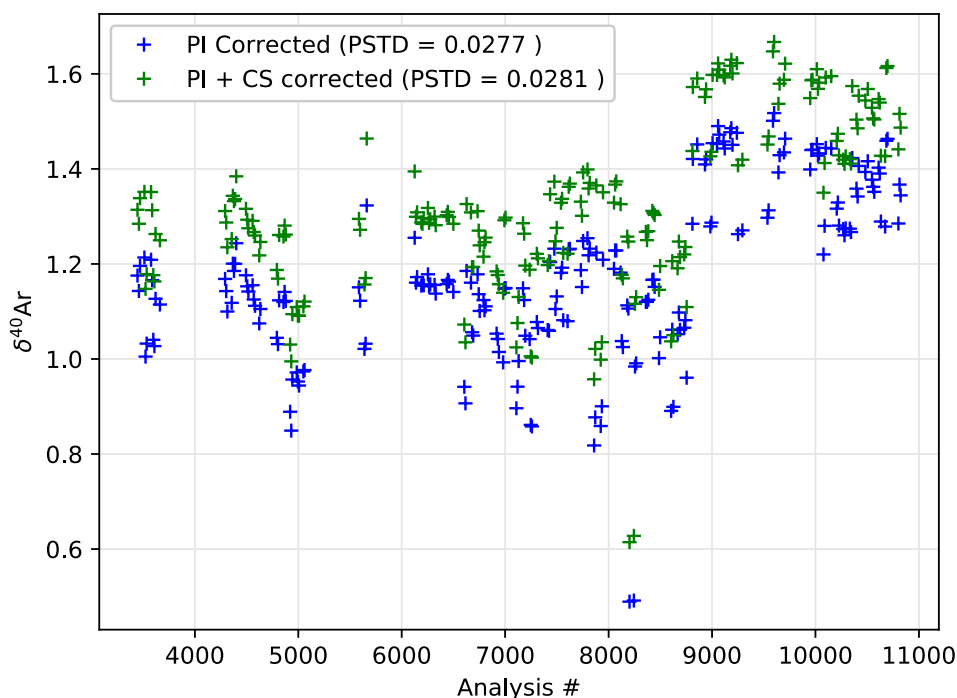
Figure A10. Correction of the chemical slope effect on δ^{40}Ar. Because the gas trapped in ice is generally argon-depleted compared to atmosphere, the chemical slope corrected values (green) are greater than non-corrected values (blue). Pooled Standard Deviation (PSTD) of each series are indicated in the captions.

Appendix A3.3 Drift correction

In addition to previously published correction, we identified that drifts around analysis 5000, or 7200 were caused by the spectrometer focus changing over time, causing a strong variability of δ^{40}Ar and PIS. This drift could not be easily resolved because it only appeared after weeks of measurements. This issue was temporarily fixed with regular autofocus, but we needed a thorough recalibration of the focus parameters to make it more stable. Later, we fully recalibrated the spectrometer focus, causing a large change in raw δ values, both on samples and standards used for calibration (from the analysis number 8800). Fortunately, the focus changes were proportionally shifting the values of PIS and the δ^{40}Ar, and did not affect δ^{15}N values, which we attribute to nitrogen being the most abundant gas supplied to the spectrometer. To distinguish from potential pressure gradient-induced fractionation during sample preparation, which would affect both δ^{40}Ar and δ^{15}N proportionally to their mass, we removed the gravitational fractionation of δ^{40}Ar using the δ^{15}N. By doing so, the drift effect on δ^{40}Ar could be quantified against the PIS_{40Ar} as shown in Fig. A11. We define a drift slope as the non-gravitational fractionation of Ar versus the PIS_{40Ar} in Eq. 5.

$$\text{Drift}_{40_{Ar}} = \frac{\Delta(\delta^{40}Ar_{CS\ corrected} - 4 \cdot \delta^{15}N_{PI\ corrected})}{\Delta PIS_{40_{Ar}}} \tag{5}$$

Using the drift slope, we then correct δ^{40}Ar values:

$$\delta^{40}\mathrm{Ar}_{\text{drift corrected}} = \delta^{40}\mathrm{Ar}_{\text{CS corrected}} - \mathrm{Drift}_{^{40}\mathrm{Ar}} \times \mathrm{PIS}_{^{40}\mathrm{Ar}} \tag{6}$$

This improved the precision as attested by PSTD of δ^{40}Ar in replicates that dropped from 0.028 ‰ to 0.013 ‰ (Fig. A12). Note that if we apply the drift correction without the chemical slope correction, the PSTD only improves to 0.016 ‰ (not shown), showing the importance of chemical slope correction prior to the drift correction.
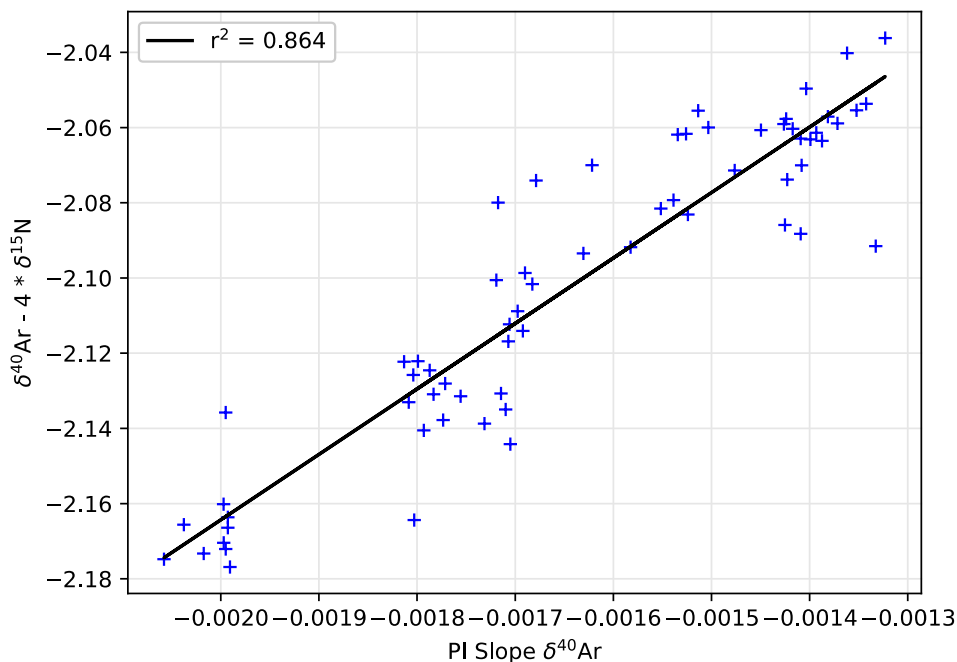
785

Figure A11. Non-gravitational fractionation of argon as a function of the PIS for argon.
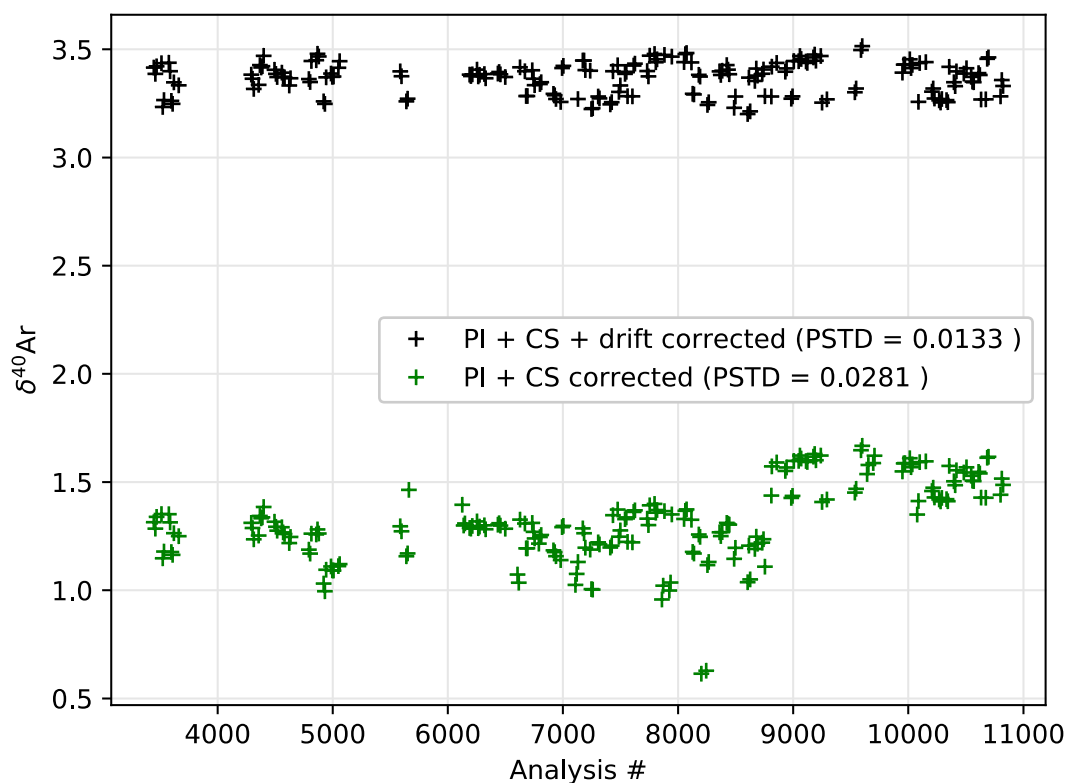
41

Figure A12. Correction of the drift effect on δ^{40}Ar. Pooled Standard Deviation (PSTD) of each series are indicated in the captions.

790 **Appendix A3.4 Normalization to atmosphere**

All δ values are defined as the relative difference to a standard. For argon and nitrogen gases, the standard is the atmospheric air (IAEA, 1995). Two to three Air standards were prepared weekly from a bottle of air captured in Saclay in 2019. The same sample preparation and corrections are applied to the Air standard, as would be made for gas extracted from an ice sample. In total, 83 replicates of Air standards were measured, with a standard deviation after all corrections of 0.0052 ‰ for δ^{15}N,

795 0.0188 ‰ for δ^{40}Ar, and 0.0029 ‰ for ^{15}N$_{excess}$. We believe that some of the error in the δ^{15}N and δ^{40}Ar is due to the sampling processing in gas line, with gas being released into empty tubing, causing large pressure differences that are known to fractionate the isotopes. Even though we try to allow some time to equilibrate, a small fractionation probably remains. This affects the two sample replicates differently because they are processed separately, but both nitrogen and argon in the same sample are affected by the same pressure changes and resulting fractionation. Given that ^{15}N$_{excess}$ is defined as the mass-

800 weighted difference between the two isotopic ratios, some of the fractionation induced by sample processing may cancel out, and therefore the difference in ^{15}N$_{excess}$ between the two samples is smaller than δ^{15}N or δ^{40}Ar alone

Climate
of the Past
Discussions

We use weekly averages of two to three measurements of $\delta^{15}N$ and $\delta^{40}Ar$ in atmospheric air to normalize the ice measurements of the corresponding week (Fig. A13). By doing this correction weekly, we further correct any drift that can happen, as it would affect both our gas trapped in ice and atmospheric air standards in the same manner.
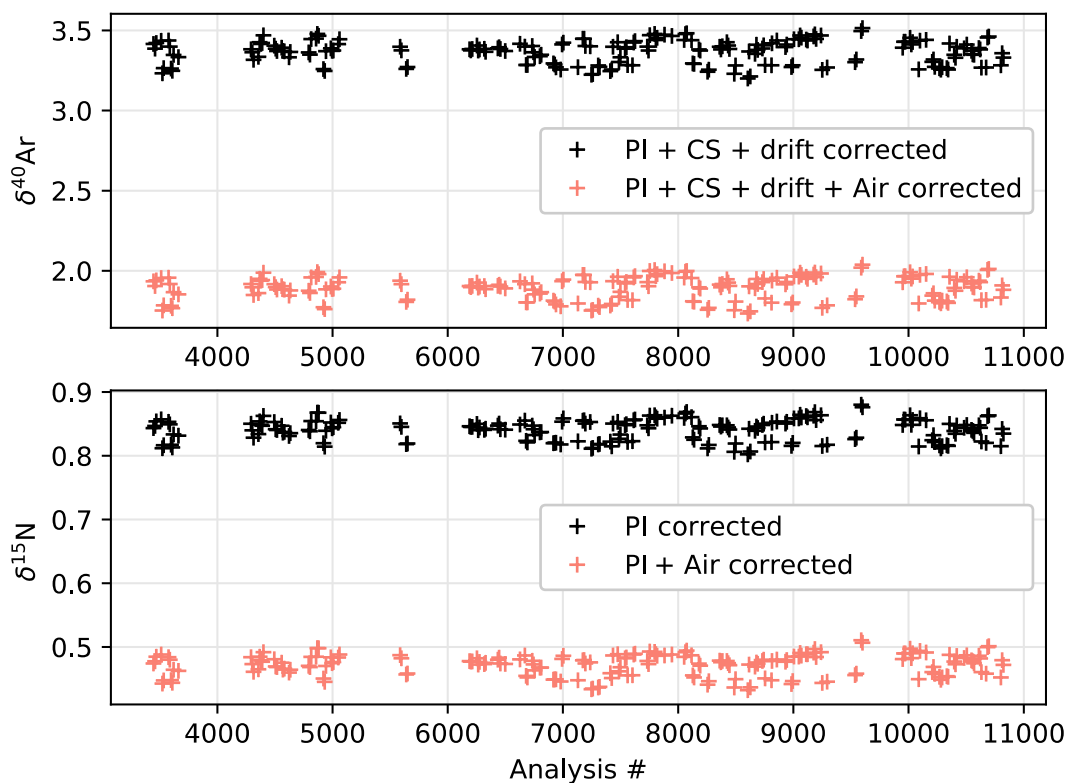
805

Figure A13. Normalization to atmosphere. The values are subsequently given in ‰ versus atmosphere. Pooled Standard Deviation is unchanged with normalization because the same correction is applied for both duplicates.

Normalization of the $\delta^{40}Ar$ and $\delta^{15}N$ of ice samples does not change the pooled standard deviation, because the two replicates are corrected by the same amount. However, it corrects the absolute value needed for quantification of gravitational and thermal

810 effects.

Appendix A4 Advection-diffusion ice model tuning

Appendix A4.1 Parameters

The model simulates the diffusion and advection of temperature in the ice. Given an initial state, the temperature will diffuse depending on boundary conditions such as surface temperature, advection due to accumulation of ice, compaction, bottom

815 temperature. We set the compaction to follow the ice density profile measured in the core, under the assumption that it did not change significantly in the past. Surface temperature is inferred from different temperature scenarios, plus a sinusoidal seasonal

Climate
of the Past
Discussions

cycle which amplitude of 13.7°C has been deduced from the temperature cycle at the ABN Automatic Weather Station. Bottom temperature is constrained by a constant geothermal heat flux of 65 mW m^{-2} for Aurora Basin (Maule, 2005; Martos et al., 2017). Temperature diffusion simulations start at 2000 BCE and last for 4014 years, allowing for flexibility in the first ~2000

820   years where we have no gas constraints. For the past 2700 years (700 BCE onwards), we use the accumulation obtained with annual layer counting with a 20-year running average (as shown in Supp. Fig. 3). Previous this date, we use the average accumulation of 94 kg m^2 a^{-1} (Akers et al., 2022). The model is also highly dependent on the initial temperature profile in the ice.

The ice thickness is suspected to have varied over time both spatially and temporally. Upstream ABN coring location, the ice

825   about is 500 m thicker than the current 3500 m, mainly because bedrock is deeper in the central part of Aurora Basin. We assume that temporal variations of ice thickness in Aurora Basin during the past 4000 years are much smaller than this. For simplification, we use an averaged thickness of 3700 m over the past 4000 years. Changes of ice thickness of 500 m caused by a surface change of accumulation may affect the temperature gradient in the upper ice column (Morgan et al., 2022), but thickness changes associated with glacial flow should not have a significant impact at the scale of 2000 years, because most

830   of the ice deformation occurs at depth (Wang and Warner, 1999; Doyle et al., 2018), and equilibration time between the bedrock and the surface is of the order of magnitude of 10,000 years. The accumulation history used in the model is inferred from the ice core accumulation with a 20-year smoothing.

Finally, the diffusion model outputs gradients of temperature between the surface and a lock-in depth, which is inferred from the lock-in depth history determined in Sect. 3.2 of main article. Uncertainties of ± 4 m in the lock-in depth result in ± 0.03°C

835   in the surface to lock-in depth temperature gradient, ten times smaller than the uncertainties on the ΔT estimated from the gases.

Appendix A4.2 Initialization with consideration of ice flow

We account for long-term influence of ABN site displacement on the temperature scenarios using a transient state initialization. Most deformations associated with ice flow occur in the bottom layers of ice in contact with the rocks, where the temperature

840   is near melting point (Wang and Warner, 1999; Doyle et al., 2018). The uppermost column of ice is advected rather uniformly, so we can consider simply consider surface temperature changes from a Lagrangian point of view, where we follow the column of ice under ABN as it flows. Therefore, we consider two components of temperature changes: spatial temperature changes due to the displacement of ice, and climatic temperature changes. For simplification, and because our simulation only spans the last 4000 years, we consider the surface topography as constant, and assume that climatic temperature changes vary

845   homogeneously spatially in the range of 40 km. This allows us to simply run the diffusion-advection model with a single dimension (depth).

We chose to initialize the model with a transient-state profile rather than a stationary temperature profile to simulate the presence of cold ice advected under ABN coring site, and better match the −2.5°C temperature gradient observed in the

borehole measurement. The initialization is performed with a transient state temperature simulation, in which we equilibrated

850   the ice column with a surface temperature of −61°C for 20,000 years and then simulate the deglaciation and the Holocene with

the temperature history from Dome C (Jouzel et al., 2007) and ice-flow related temperature changes from modern surface

temperature (Agosta et al., 2019) and ice flow velocities (Mouginot et al., 2019). The temperature history used during

initialization is shown in Fig. A14. The initialization run is unique and starts from 30,000 BCE to 2,000 BCE. The past

accumulation during initialization is set at 40 % of the average ABN accumulation, increasing to 80 % during deglaciation and

855   ramping up to 100 % at 2,000 BCE. The ratio of accumulation between the last glacial maximum and the late Holocene is set

to be roughly the same as Dome C (Wolff et al., 2010) and WAIS Divide (Buizert et al., 2015). Arguably, the ice-flow was

slower than modern day in the glacial period, which would result in smaller temperature changes if modelled correctly, but

such precision is not needed in the initialization of the model. This transient initialization produces a temperature profile with

a strong gradient, which can match the observations within 0.5°C if the simulation is continued until 2014 CE (Fig. A15), and

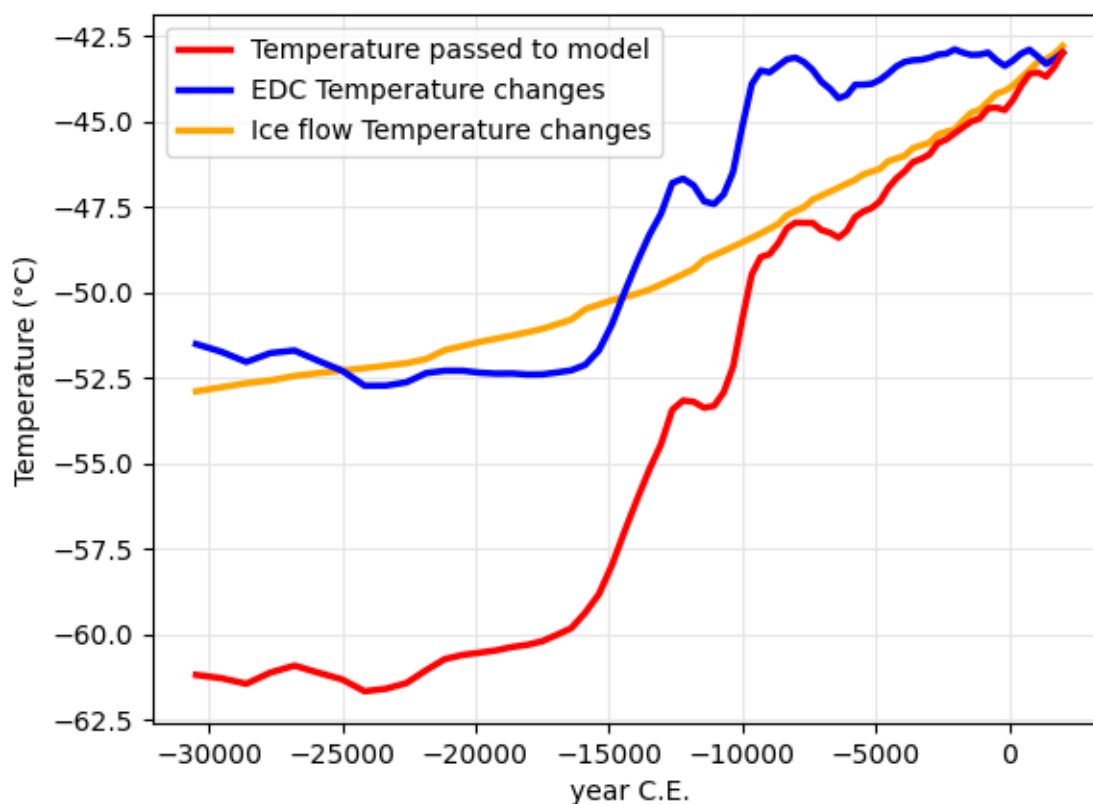860   is thus a good starting point for the temperature simulations.

Figure A14. Base surface temperature passed to the model in the transient state initialization, which runs from 30,000 BCE to 2000 BCE, and the unperturbed simulation from 2000 BCE to 2014 CE. Red line shows the total temperature changes, blue line shows

Climate
of the Past

Open Access

Discussions

EGU

EDC temperature changes (Jouzel et al., 2007; shifted to match ABN modern temperature) and orange line shows the ice-flow related
865   **temperature changes from a simple interpolation of modern-day Antarctic surface temperature along the estimated back-projected**
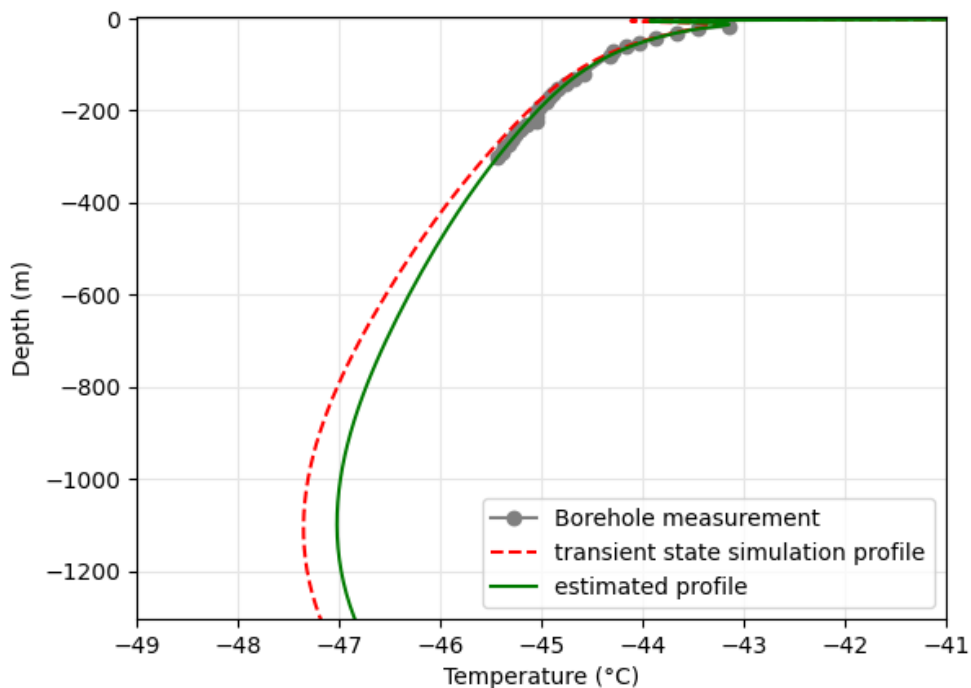**position of ABN using modern flow speeds (Mouginot et al., 2019).**

Figure A15. Temperature profile obtained after the transient state initialization (red dotted line), as compared to the borehole
temperature profile (grey) and the estimated temperature profile after inversion (green).

870   **Appendix A4.3 Temperature perturbation simulations**

Starting from the transient state profile of temperature at 2000 BCE, we start simulations following the same base surface
temperature forcing (later part of Fig. A14), and add a "triangle" shaped perturbation in each simulation, with an additional
temperature increase ramping up to +1°C. The added perturbation increases over the course of 10 years then decreases in
another 10 years to return to the base surface temperature forcing for the remainder of the simulation. The next simulation uses
875   a perturbation that is shifted in the time by 10 years. A few longer lasting perturbations are used in the 2000 BCE – 0 CE
period, where the constraints are low because of the absence of gas data, and the climate information is not used in the results
of this study. We perform a total of 220 simulations with perturbations at different times in the run.

Appendix A5 Parameters of the temperature inversion
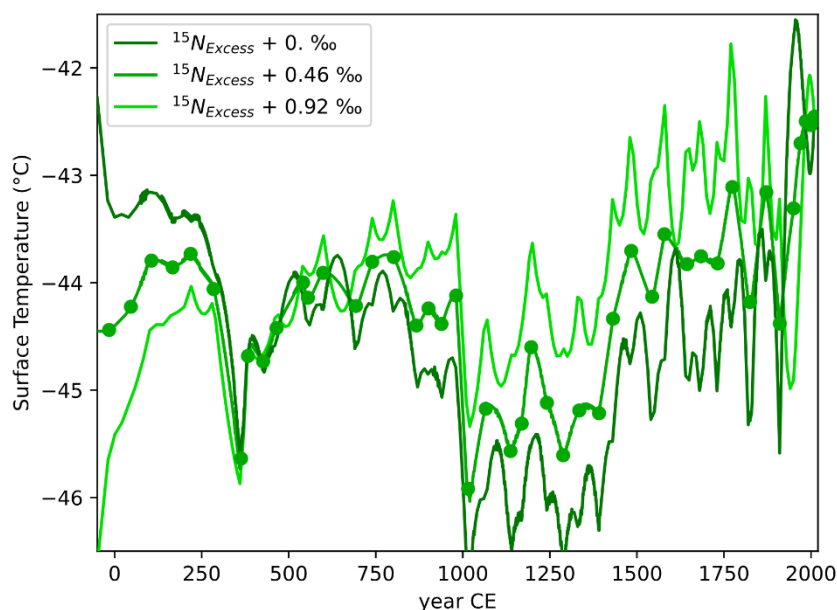
880 **Appendix A5.1 Shift of the $^{15}N_{excess}$ mean value**

Figure A16. History of temperature obtained with inversion of borehole and temperature gradients obtained with $^{15}N_{excess}$, using different correction values for $^{15}N_{excess}$. Not correcting or correcting too strongly the $^{15}N_{excess}$ causes the temperature reconstruction to squeeze fast saw-tooth shaped variations between ages where we have gases datapoints, represented by the dots.
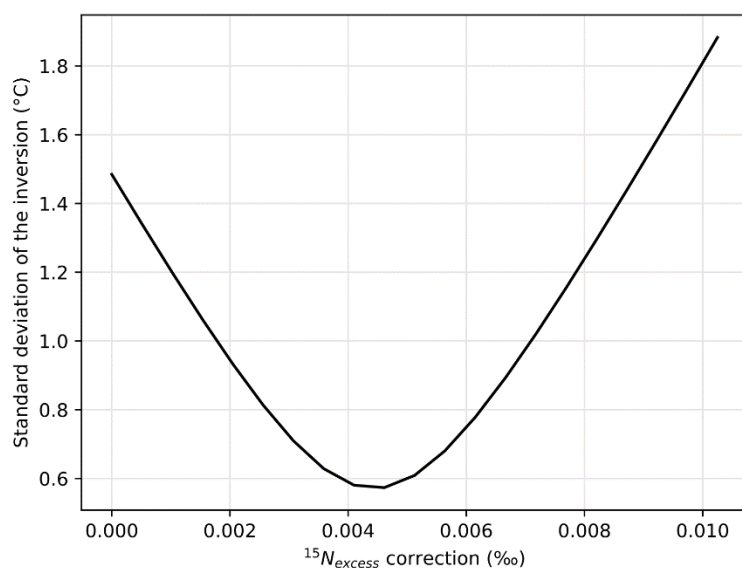
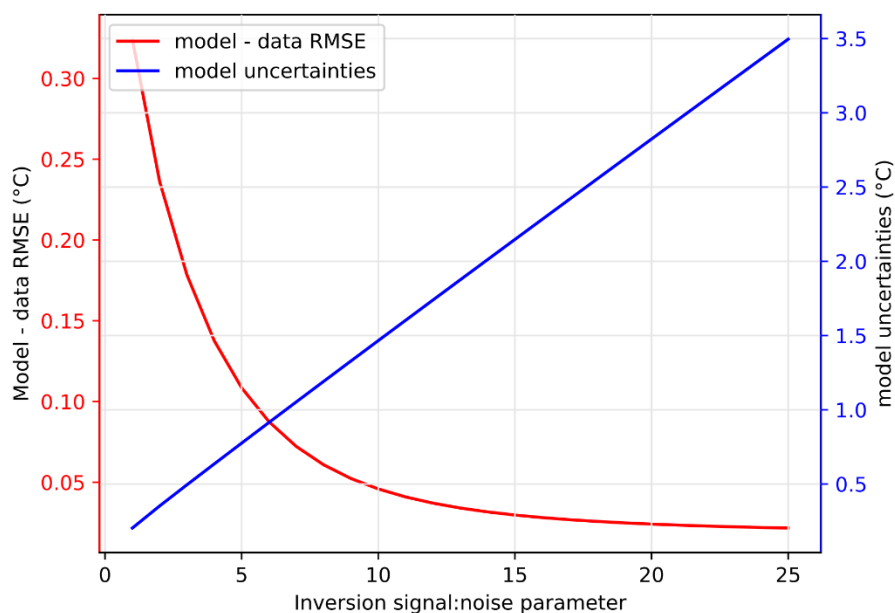885

Figure A17. Standard deviation of the history of temperature depending on the value used for $^{15}N_{excess}$ correction. A value of 0.0046 ‰ is best to minimize the intrinsic variability of the reconstruction and match both datasets.

47

Climate
of the Past
Discussions

Appendix A5.2 Uncertainty parameters

Figure A18. Root Mean Square Error (RMSE, red) between temperature reconstruction and temperature data passed to the inversion, and reconstruction uncertainty (blue) as a function of signal to noise parameter. A signal to noise ratio too low results in a too smooth inversion with high model-data mismatch, whereas a too high parameter increases the resulting inversion uncertainty to allow all for more flexibility
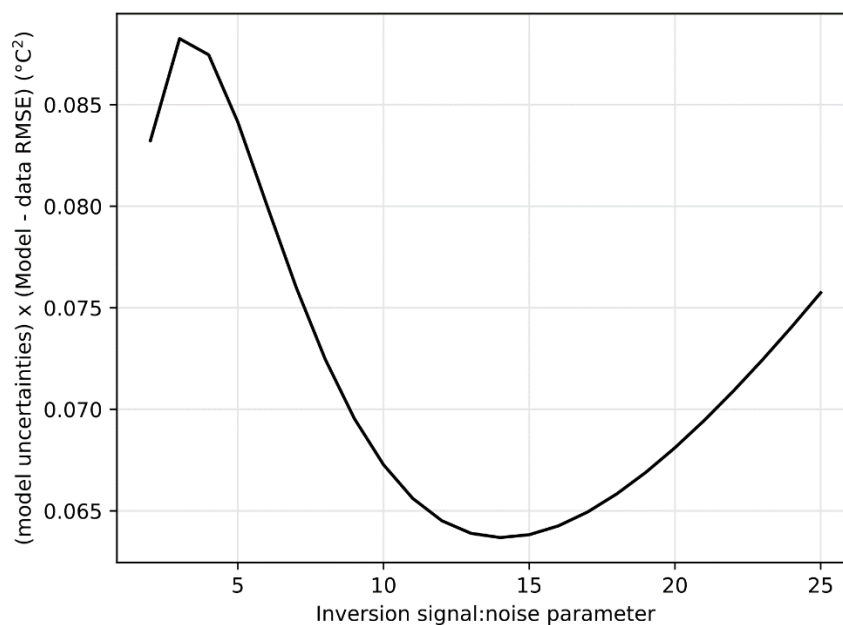
Figure A19. Cost-function of the reconstruction as a function of signal to noise parameter used in the inversion. A value of 14 is best to ensure that the inversion matches the constraints and minimize its uncertainty.

Appendix A5.3 Age significance of data points in the reconstruction

The diffusion of temperature in the firn depends both on snow and ice properties but also the accumulation rate at the ice core site. At West Antarctic Ice Sheet Divide (WAIS Divide), the temperature measured at depths corresponding to the last

900 millennium was estimated to integrate temperature with a smoothing window of several hundred years (Orsi et al., 2012); for ABN where the ice accumulation is half as high as WAIS Divide, we expect even greater smoothing windows. The temporal range of temperature changes recorded by $^{15}N_{excess}$ at ABN is limited at the minimum by the diffusion time of gases between the surface and the lock-in zone, and at maximum by the smoothing out of the temperature gradient by the temperature diffusion in the ice column. At NEEM, gases take on average 10 years to diffuse down to the lock-in depth of 63 m (Witrant et al.,

905 2012); we expect that at ABN, where the lock-in depth is about 30 m deeper, the gases will take slightly longer to equilibrate in the diffusive column, so a temperature gradient maintained approximately 20 years should be effectively recorded in the $^{15}N_{excess}$.

In addition, we further reduced the time-resolution of gas-based reconstruction by averaging the isotopic values in 5 m windows, with an expected age range of about 45 years. Lastly, we applied a smoothing in the inversion to limit the variability

910 of neighbouring points by forcing a covariance in the reconstruction. The covariance parameter was set to be exponentially decreasing with age difference, with a 0.5 covariance reached at 70 years difference. Therefore, the reconstruction includes multiple gas data points for each inversion point, strengthening the confidence in the reconstructed temperature. In our figures, we chose to represent the inversion at the time-resolution of points when there is a gas-based temperature constraint.

915 **Data availability**

Water isotope ($\delta^{18}O$ and δD), gas isotope ($\delta^{15}N$ and $\delta^{40}Ar$), borehole temperature data, as well as temperature reconstructions will be accessible in a repository on the Australian Antarctic Division data centre website (https://data.gov.au/ – full link will be available upon acceptation of the present manuscript).

Author contribution

920 MC directed the ABN ice core drilling project. AO and AS designed the study. Raw water isotope data was measured and curated by AM. AO designed the gas isotope analysis, AS performed the gas isotope analysis. TP measured the borehole temperature. AO secured financial resources for gas laboratory analyses and, together with AL, supervised stable isotope interpretations. JMC measured water stable isotopes in the short core used for calibration. JMC, XF and JC measured the methane used for gas age model. ELM provided upstream GPS elevation profiles and radar reflector surfaces. CP performed

925 the annual layer counting, MC provided volcanic tie ages for ice age model. AO adapted the ice diffusion model and designed the inversion algorithm. AS performed the diffusion model simulations. AS and AO interpreted the climate implications of the

results. AS wrote the original draft and created the figures. AP, AJ, MC, AM, AL, JMC, ELM, XF, and JC contributed to the review of the manuscript.

Competing interests

930   The authors declare that they have no conflict of interest.

References

Abram, N. J., Mulvaney, R., Vimeux, F., Phipps, S. J., Turner, J., and England, M. H.: Evolution of the Southern Annular Mode during the past millennium, Nature Clim Change, 4, 564–569, https://doi.org/10.1038/nclimate2235, 2014.

940   Abram, N. J., McGregor, H. V., Tierney, J. E., Evans, M. N., McKay, N. P., and Kaufman, D. S.: Early onset of industrial-era warming across the oceans and continents, Nature, 536, 411–418, https://doi.org/10.1038/nature19082, 2016.

Agosta, C., Amory, C., Kittel, C., Orsi, A. J., Favier, V., Gallée, H., van den Broeke, M. R., Lenaerts, J. T. M., van Wessem, J. M., van de Berg, W. J., and Fettweis, X.: Estimation of the Antarctic surface mass balance using the regional climate model MAR (1979–2015) and identification of dominant processes, The Cryosphere, 13, 281–296, https://doi.org/10.5194/tc-13-281-945   2019, 2019.

Akers, P. D., Savarino, J., Caillon, N., Servettaz, A. P. M., Le Meur, E., Magand, O., Martins, J., Agosta, C., Crockford, P., Kobayashi, K., Hattori, S., Curran, M., van Ommen, T., Jong, L., and Roberts, J. L.: Sunlight-driven nitrate loss records Antarctic surface mass balance, Nat Commun, 13, 1–10, https://doi.org/10.1038/s41467-022-31855-7, 2022.

Bereiter, B., Kawamura, K., and Severinghaus, J. P.: New methods for measuring atmospheric heavy noble gas isotope and 950   elemental ratios in ice core samples, Rapid Commun Mass Spectrom, 32, 801–814, https://doi.org/10.1002/rcm.8099, 2018.

Bertler, N. A. N., Conway, H., Dahl-Jensen, D., Emanuelsson, D. B., Winstrup, M., Vallelonga, P. T., Lee, J. E., Brook, E. J., Severinghaus, J. P., Fudge, T. J., Keller, E. D., Baisden, W. T., Hindmarsh, R. C. A., Neff, P. D., Blunier, T., Edwards, R., Mayewski, P. A., Kipfstuhl, S., Buizert, C., Canessa, S., Dadic, R., Kjær, H. A., Kurbatov, A., Zhang, D., Waddington, E. D., Baccolo, G., Beers, T., Brightley, H. J., Carter, L., Clemens-Sewall, D., Ciobanu, V. G., Delmonte, B., Eling, L., Ellis, A., 955   Ganesh, S., Golledge, N. R., Haines, S., Handley, M., Hawley, R. L., Hogan, C. M., Johnson, K. M., Korotkikh, E., Lowry, D. P., Mandeno, D., McKay, R. M., Menking, J. A., Naish, T. R., Noerling, C., Ollive, A., Orsi, A. J., Proemse, B. C., Pyne, A. R., Pyne, R. L., Renwick, J., Scherer, R. P., Semper, S., Simonsen, M., Sneed, S. B., Steig, E. J., Tuohy, A., Venugopal, A. U., Valero-Delgado, F., Venkatesh, J., Wang, F., Wang, S., Winski, D. A., Winton, V. H. L., Whiteford, A., Xiao, C., Yang,

J., and Zhang, X.: The Ross Sea Dipole – temperature, snow accumulation and sea ice variability in the Ross Sea region,
960 Antarctica, over the past 2700 years, Clim. Past, 14, 193–214, https://doi.org/10.5194/cp-14-193-2018, 2018.

Buizert, C. and Severinghaus, J. P.: Dispersion in deep polar firn driven by synoptic-scale surface pressure variability, The
Cryosphere, 10, 2099–2111, https://doi.org/10.5194/tc-10-2099-2016, 2016.

Buizert, C., Martinerie, P., Petrenko, V. V., Severinghaus, J. P., Trudinger, C. M., Witrant, E., Rosen, J. L., Orsi, A. J., Rubino,
M., Etheridge, D. M., Steele, L. P., Hogan, C., Laube, J. C., Sturges, W. T., Levchenko, V. A., Smith, A. M., Levin, I., Conway,
965 T. J., Dlugokencky, E. J., Lang, P. M., Kawamura, K., Jenk, T. M., White, J. W. C., Sowers, T., Schwander, J., and Blunier,
T.: Gas transport in firn: multiple-tracer characterisation and model intercomparison for NEEM, Northern Greenland, Atmos.
Chem. Phys., 12, 4259–4277, https://doi.org/10.5194/acp-12-4259-2012, 2012.

Buizert, C., Cuffey, K. M., Severinghaus, J. P., Baggenstos, D., Fudge, T. J., Steig, E. J., Markle, B. R., Winstrup, M., Rhodes,
R. H., Brook, E. J., Sowers, T. A., Clow, G. D., Cheng, H., Edwards, R. L., Sigl, M., McConnell, J. R., and Taylor, K. C.: The
970 WAIS Divide deep ice core WD2014 chronology – Part 1: Methane synchronization (68–31 ka BP) and the gas age–ice age
difference, Clim. Past, 11, 153–173, https://doi.org/10.5194/cp-11-153-2015, 2015.

Buizert, C., Fudge, T. J., Roberts, W. H. G., Steig, E. J., Sherriff-Tadano, S., Ritz, C., Lefebvre, E., Edwards, J., Kawamura,
K., Oyabu, I., Motoyama, H., Kahle, E. C., Jones, T. R., Abe-Ouchi, A., Obase, T., Martin, C., Corr, H., Severinghaus, J. P.,
Beaudette, R., Epifanio, J. A., Brook, E. J., Martin, K., Chappellaz, J., Aoki, S., Nakazawa, T., Sowers, T. A., Alley, R. B.,
975 Ahn, J., Sigl, M., Severi, M., Dunbar, N. W., Svensson, A., Fegyveresi, J. M., He, C., Liu, Z., Zhu, J., Otto-Bliesner, B. L.,
Lipenkov, V. Y., Kageyama, M., and Schwander, J.: Antarctic surface temperature and elevation during the Last Glacial
Maximum, Science, 372, 1097–1101, https://doi.org/10.1126/science.abd2897, 2021.

Casado, M., Orsi, A. J., and Landais, A.: On the limits of climate reconstruction from water stable isotopes in polar ice cores,
PAGES Mag, 25, 146–147, https://doi.org/10.22498/pages.25.3.146, 2017.

980 Casado, M., Landais, A., Picard, G., Münch, T., Laepple, T., Stenni, B., Dreossi, G., Ekaykin, A., Arnaud, L., Genthon, C.,
Touzeau, A., Masson-Delmotte, V., and Jouzel, J.: Archival processes of the water stable isotope signal in East Antarctic ice
cores, The Cryosphere, 12, 1745–1766, https://doi.org/10.5194/tc-12-1745-2018, 2018.

Casado, M., Münch, T., and Laepple, T.: Climatic information archived in ice cores: impact of intermittency and diffusion on
the recorded isotopic signal in Antarctica, Clim. Past, 16, 1581–1598, https://doi.org/10.5194/cp-16-1581-2020, 2020.

985 Christiansen, B. and Ljungqvist, F. C.: Challenges and perspectives for large-scale temperature reconstructions of the past two
millennia, Reviews of Geophysics, 55, 40–96, https://doi.org/10.1002/2016RG000521, 2017.

Ciais, P. and Jouzel, J.: Deuterium and oxygen 18 in precipitation: Isotopic model, including mixed cloud processes, J.
Geophys. Res., 99, 16793, https://doi.org/10.1029/94JD00412, 1994.

Cole-Dai, J., Mosley-Thompson, E., Wight, S. P., and Thompson, L. G.: A 4100-year record of explosive volcanism from an
990 East Antarctica ice core, J. Geophys. Res., 105, 24431–24441, https://doi.org/10.1029/2000JD900254, 2000.

Craig, H., Horibe, Y., and Sowers, T.: Gravitational Separation of Gases and Isotopes in Polar Ice Caps, Science, 242, 1675–
1678, https://doi.org/10.1126/science.242.4886.1675, 1988.

Crosta, X., Etourneau, J., Orme, L. C., Dalaiden, Q., Campagne, P., Swingedouw, D., Goosse, H., Massé, G., Miettinen, A.,
McKay, R. M., Dunbar, R. B., Escutia, C., and Ikehara, M.: Multi-decadal trends in Antarctic sea-ice extent driven by ENSO–
995 SAM over the last 2,000 years, Nat. Geosci., https://doi.org/10.1038/s41561-021-00697-1, 2021.

51

Cuffey, K. M., Clow, G. D., Alley, R. B., Stuiver, M., Waddington, E. D., and Saltus, R. W.: Large Arctic Temperature Change at the Wisconsin-Holocene Glacial Transition, Science, 270, 455–458, https://doi.org/10.1126/science.270.5235.455, 1995.

Dahl-Jensen, D., Mosegaard, K., Gundestrup, N., Clow, G. D., Johnsen, S. J., Hansen, A. W., and Balling, N.: Past Temperatures Directly from the Greenland Ice Sheet, Science, 282, 268–271, https://doi.org/10.1126/science.282.5387.268, 1000   1998.

Dansgaard, W.: Stable isotopes in precipitation, Tellus, 16, 436–468, https://doi.org/10.1111/j.2153-3490.1964.tb00181.x, 1964.

Dätwyler, C., Neukom, R., Abram, N. J., Gallant, A. J. E., Grosjean, M., Jacques-Coper, M., Karoly, D. J., and Villalba, R.: Teleconnection stationarity, variability and trends of the Southern Annular Mode (SAM) during the last millennium, Clim 1005   Dyn, 51, 2321–2339, https://doi.org/10.1007/s00382-017-4015-0, 2018.

Doyle, S. H., Hubbard, B., Christoffersen, P., Young, T. J., Hofstede, C., Bougamont, M., Box, J. E., and Hubbard, A.: Physical Conditions of Fast Glacier Flow: 1. Measurements From Boreholes Drilled to the Bed of Store Glacier, West Greenland, J. Geophys. Res. Earth Surf., 123, 324–348, https://doi.org/10.1002/2017JF004529, 2018.

Fogt, R. L. and Marshall, G. J.: The Southern Annular Mode: Variability, trends, and climate impacts across the Southern 1010   Hemisphere, WIREs Clim Change, 11, https://doi.org/10.1002/wcc.652, 2020.

Fogt, R. L., Perlwitz, J., Monaghan, A. J., Bromwich, D. H., Jones, J. M., and Marshall, G. J.: Historical SAM Variability. Part II: Twentieth-Century Variability and Trends from Reconstructions, Observations, and the IPCC AR4 Models, Journal of Climate, 22, 5346–5365, https://doi.org/10.1175/2009JCLI2786.1, 2009.

Fourteau, K., Martinerie, P., Fain, X., Schaller, C. F., Tuckwell, R. J., Löwe, H., Arnaud, L., Magand, O., Thomas, E. R., 1015   Freitag, J. H., Mulvaney, R., Schneebeli, M., and Lipenkov, V. Y.: Multi-tracer study of gas trapping in an East Antarctic ice core, The Cryosphere, 13, 3383–3403, https://doi.org/10.5194/tc-2019-89, 2019.

Goujon, C., Barnola, J.-M., and Ritz, C.: Modeling the densification of polar firn including heat diffusion: Application to close-off characteristics and gas isotopic fractionation for Antarctica and Greenland sites: A NEW FIRN DENSIFICATION MODEL, J. Geophys. Res., 108, n/a-n/a, https://doi.org/10.1029/2002JD003319, 2003.

1020   Goursaud, S., Masson-Delmotte, V., Favier, V., Orsi, A. J., and Werner, M.: Water stable isotope spatio-temporal variability in Antarctica in 1960–2013: observations and simulations from the ECHAM5-wiso atmospheric general circulation model, Clim. Past, 14, 923–946, https://doi.org/10.5194/cp-14-923-2018, 2018.

Grachev, A. M. and Severinghaus, J. P.: Determining the Thermal Diffusion Factor for 40Ar/36Ar in Air To Aid Paleoreconstruction of Abrupt Climate Change, J. Phys. Chem. A, 107, 4636–4642, https://doi.org/10.1021/jp027817u, 2003.

1025   Hudson, S. R. and Brandt, R. E.: A Look at the Surface-Based Temperature Inversion on the Antarctic Plateau, Journal of Climate, 18, 1673–1696, https://doi.org/10.1175/JCLI3360.1, 2005.

IAEA: Reference and intercomparison materials for stable isotopes of light elements. Proceedings of a consultants meeting held in Vienna, 1-3 December 1993, International Atomic Energy Agency, 1995.

Johnsen, S. J., Dahl-Jensen, D., Dansgaard, W., and Gundestrup, N.: Greenland palaeotemperatures derived from GRIP bore 1030   hole temperature and ice core isotope profiles, Tellus B, 47, 624–629, https://doi.org/10.1034/j.1600-0889.47.issue5.9.x, 1995.

Jones, J. M., Gille, S. T., Goosse, H., Abram, N. J., Canziani, P. O., Charman, D. J., Clem, K. R., Crosta, X., de Lavergne, C., Eisenman, I., England, M. H., Fogt, R. L., Frankcombe, L. M., Marshall, G. J., Masson-Delmotte, V., Morrison, A. K., Orsi, A. J., Raphael, M. N., Renwick, J. A., Schneider, D. P., Simpkins, G. R., Steig, E. J., Stenni, B., Swingedouw, D., and Vance, T. R.: Assessing recent trends in high-latitude Southern Hemisphere surface climate, Nature Clim Change, 6, 917–926, https://doi.org/10.1038/nclimate3103, 2016.

Jones, P. D., Briffa, K. R., Osborn, T. J., Lough, J. M., van Ommen, T. D., Vinther, B. M., Luterbacher, J., Wahl, E. R., Zwiers, F. W., Mann, M. E., Schmidt, G. A., Ammann, C. M., Buckley, B. M., Cobb, K. M., Esper, J., Goosse, H., Graham, N., Jansen, E., Kiefer, T., Kull, C., Küttel, M., Mosley-Thompson, E., Overpeck, J. T., Riedwyl, N., Schulz, M., Tudhope, A. W., Villalba, R., Wanner, H., Wolff, E., and Xoplaki, E.: High-resolution palaeoclimatology of the last millennium: a review of current status and future prospects, The Holocene, 19, 3–49, https://doi.org/10.1177/0959683608098952, 2009.

Jouzel, J. and Merlivat, L.: Deuterium and oxygen 18 in precipitation: Modeling of the isotopic effects during snow formation, J. Geophys. Res., 89, 11749, https://doi.org/10.1029/JD089iD07p11749, 1984.

Jouzel, J., Alley, R. B., Cuffey, K. M., Dansgaard, W., Grootes, P., Hoffmann, G., Johnsen, S. J., Koster, R. D., Peel, D., Shuman, C. A., Stievenard, M., Stuiver, M., and White, J.: Validity of the temperature reconstruction from water isotopes in ice cores, J. Geophys. Res., 102, 26471–26487, https://doi.org/10.1029/97JC01283, 1997.

Jouzel, J., Vimeux, F., Caillon, N., Delaygue, G., Hoffmann, G., Masson-Delmotte, V., and Parrenin, F.: Magnitude of isotope/temperature scaling for interpretation of central Antarctic ice cores, Journal of Geophysical Research: Atmospheres, 108, 4361–4372, https://doi.org/10.1029/2002JD002677, 2003.

Jouzel, J., Masson-Delmotte, V., Cattani, O., Dreyfus, G., Falourd, S., Hoffmann, G., Minster, B., Nouet, J., Barnola, J. M., Chappellaz, J., Fischer, H., Gallet, J. C., Johnsen, S. J., Leuenberger, M., Loulergue, L., Luethi, D., Oerter, H., Parrenin, F., Raisbeck, G., Raynaud, D., Schilt, A., Schwander, J., Selmo, E., Souchez, R., Spahni, R., Stauffer, B., Steffensen, J. P., Stenni, B., Stocker, T. F., Tison, J. L., Werner, M., and Wolff, E. W.: Orbital and Millennial Antarctic Climate Variability over the Past 800,000 Years, Science, 317, 793–796, https://doi.org/10.1126/science.1141038, 2007.

Kawamura, K., Severinghaus, J. P., Albert, M. R., Courville, Z. R., Fahnestock, M. A., Scambos, T., Shields, E., and Shuman, C. A.: Kinetic fractionation of gases by deep air convection in polar firn, Atmos. Chem. Phys., 13, 11141–11155, https://doi.org/10.5194/acp-13-11141-2013, 2013.

Kobashi, T., Severinghaus, J. P., and Kawamura, K.: Argon and nitrogen isotopes of trapped air in the GISP2 ice core during the Holocene epoch (0–11,500 B.P.): Methodology and implications for gas loss processes, Geochimica et Cosmochimica Acta, 72, 4675–4686, https://doi.org/10.1016/j.gca.2008.07.006, 2008.

Koffman, B. G., Kreutz, K. J., Breton, D. J., Kane, E. J., Winski, D. A., Birkel, S. D., Kurbatov, A. V., and Handley, M. J.: Centennial-scale variability of the Southern Hemisphere westerly wind belt in the eastern Pacific over the past two millennia, Climate of the Past, 10, 1125–1144, https://doi.org/10.5194/cp-10-1125-2014, 2014.

Landais, A., Casado, M., Prié, F., Magand, O., Arnaud, L., Ekaykin, A., Petit, J.-R., Picard, G., Fily, M., Minster, B., Touzeau, A., Goursaud, S., Masson-Delmotte, V., Jouzel, J., and Orsi, A.: Surface studies of water isotopes in Antarctica for quantitative interpretation of deep ice core data, Comptes Rendus Geoscience, 349, 139–150, https://doi.org/10.1016/j.crte.2017.05.003, 2017.

Markle, B. R. and Steig, E. J.: Improving temperature reconstructions from ice-core water-isotope records, Clim. Past, 18, 1321–1368, https://doi.org/10.5194/cp-18-1321-2022, 2022.

Marshall, G. J.: Trends in the Southern Annular Mode from Observations and Reanalyses, Journal of Climate, 16, 4134–4143,
1070 https://doi.org/10.1175/1520-0442(2003)016<4134:TITSAM>2.0.CO;2, 2003.

Marshall, G. J. and Thompson, D. W. J.: The signatures of large-scale patterns of atmospheric variability in Antarctic surface
temperatures: Antarctic Temperatures, J. Geophys. Res. Atmos., 121, 3276–3289, https://doi.org/10.1002/2015JD024665,
2016.

Marshall, G. J., Thompson, D. W. J., and Broeke, M. R.: The Signature of Southern Hemisphere Atmospheric Circulation
1075 Patterns in Antarctic Precipitation, Geophys. Res. Lett., 44, 11,580-11,589, https://doi.org/10.1002/2017GL075998, 2017.

Martos, Y. M., Catalán, M., Jordan, T. A., Golynsky, A., Golynsky, D., Eagles, G., and Vaughan, D. G.: Heat Flux Distribution
of Antarctica Unveiled, Geophys. Res. Lett., 44, 11,417-11,426, https://doi.org/10.1002/2017GL075609, 2017.

Maselli, O. J., Fritzsche, D., Layman, L., McConnell, J. R., and Meyer, H.: Comparison of water isotope-ratio determinations
using two cavity ring-down instruments and classical mass spectrometry in continuous ice-core analysis, Isotopes in
1080 Environmental and Health Studies, 49, 387–398, https://doi.org/10.1080/10256016.2013.781598, 2013.

Maule, C. F.: Heat Flux Anomalies in Antarctica Revealed by Satellite Magnetic Data, Science, 309, 464–467,
https://doi.org/10.1126/science.1106888, 2005.

McConnell, J. R., Lamorey, G. W., Lambert, S. W., and Taylor, K. C.: Continuous Ice-Core Chemical Analyses Using
Inductively Coupled Plasma Mass Spectrometry, Environ. Sci. Technol., 36, 7–11, https://doi.org/10.1021/es011088z, 2002.

1085 McMorrow, A., van Ommen, T. D., Morgan, V., and Curran, M. A. J.: Ultra-high-resolution seasonality of trace-ion species
and oxygen isotope ratios in Antarctic firn over four annual cycles, Annals of Glaciology, 39, 34–40,
https://doi.org/10.3189/172756404781814609, 2004.

Meredith, M., Sommerkorn, M., Cassotta, S., Derksen, C., Ekaykin, A., Hollowed, A., Kofinas, G., Mackintosh, A.,
Melbourne-Thomas, J., Muelbert, M. M. C., Ottersen, G., Pritchard, H., and Schuur, E. A. G.: Chapter 3: Polar Regions, in:
1090 The Ocean and Cryosphere in a Changing Climate: Special Report of the Intergovernmental Panel on Climate Change,
Cambridge University Press, https://doi.org/10.1017/9781009157964, 2022.

Mitchell, L. E., Brook, E. J., Sowers, T., McConnell, J. R., and Taylor, K.: Multidecadal variability of atmospheric methane,
1000–1800 C.E., Journal of Geophysical Research: Biogeosciences, 116, https://doi.org/10.1029/2010JG001441, 2011.

Morgan, J. D., Buizert, C., Fudge, T. J., Kawamura, K., Severinghaus, J. P., and Trudinger, C. M.: Gas isotope thermometry
1095 in the South Pole and Dome Fuji ice cores provides evidence for seasonal rectification of ice core gas records, The Cryosphere,
16, 2947–2966, https://doi.org/10.5194/tc-16-2947-2022, 2022.

Mouginot, J., Rignot, E., and Scheuchl, B.: Continent-Wide, Interferometric SAR Phase, Mapping of Antarctic Ice Velocity,
Geophys. Res. Lett., 46, 9710–9718, https://doi.org/10.1029/2019GL083826, 2019.

Moy, A., van Ommen, T., McConnel, J., Curran, M., Phipps, S., Masson-Delmotte, V., Orsi, A. J., Touzeau, A., Roberts, J.,
1100 Dahl-Jensen, D., Popp, T., Svensson, A., Landais, A., Vance, T., Liu, Y., and Arienzo, M.: Climate history at Aurora Basin
North, East Antarctica: A 2,000 year isotopic record, 19, 5821, 2017.

Münch, T. and Laepple, T.: What climate signal is contained in decadal- to centennial-scale isotope variations from Antarctic
ice cores?, Clim. Past, 14, 2053–2070, https://doi.org/10.5194/cp-14-2053-2018, 2018.

Münch, T., Kipfstuhl, S., Freitag, J., Meyer, H., and Laepple, T.: Constraints on post-depositional isotope modifications in
1105   East Antarctic firn from analysing temporal changes of isotope profiles, The Cryosphere, 11, 2175–2188,
https://doi.org/10.5194/tc-11-2175-2017, 2017.

Muto, A., Scambos, T. A., Steffen, K., Slater, A. G., and Clow, G. D.: Recent surface temperature trends in the interior of East
Antarctica from borehole firn temperature measurements and geophysical inverse methods, Geophysical Research Letters, 38,
https://doi.org/10.1029/2011GL048086, 2011.

1110   Nicolas, J. P. and Bromwich, D. H.: New Reconstruction of Antarctic Near-Surface Temperatures: Multidecadal Trends and
Reliability of Global Reanalyses, J. Climate, 27, 8070–8093, https://doi.org/10.1175/JCLI-D-13-00733.1, 2014.

Orsi, A. J.: Temperature reconstruction at the West Antarctic Ice Sheet Divide, for the last millennium, from the combination
of borehole temperature and inert gas isotope measurements, University of California, San Diego, 266 pp., 2013.

Orsi, A. J., Cornuelle, B. D., and Severinghaus, J. P.: Little Ice Age cold interval in West Antarctica: Evidence from borehole
1115   temperature at the West Antarctic Ice Sheet (WAIS) Divide: WAIS DIVIDE TEMPERATURE, Geophys. Res. Lett., 39, n/a-
n/a, https://doi.org/10.1029/2012GL051260, 2012.

Orsi, A. J., Cornuelle, B. D., and Severinghaus, J. P.: Magnitude and temporal evolution of Dansgaard–Oeschger event 8
abrupt temperature change inferred from nitrogen and argon isotopes in GISP2 ice using a new least-squares inversion, Earth
and Planetary Science Letters, 395, 81–90, https://doi.org/10.1016/j.epsl.2014.03.030, 2014.

1120   Orsi, A. J., Kawamura, K., Masson-Delmotte, V., Fettweis, X., Box, J. E., Dahl-Jensen, D., Clow, G. D., Landais, A., and
Severinghaus, J. P.: The recent warming trend in North Greenland, Geophysical Research Letters, 44, 6235–6243,
https://doi.org/10.1002/2016GL072212, 2017.

PAGES 2k Consortium: Continental-scale temperature variability during the past two millennia, Nature Geoscience, 6, 339–
346, https://doi.org/10.1038/ngeo1797, 2013.

1125   Pang, H., Hou, S., Landais, A., Masson-Delmotte, V., Prie, F., Steen-Larsen, H. C., Risi, C., Li, Y., Jouzel, J., Wang, Y., He,
J., Minster, B., and Falourd, S.: Spatial distribution of 17O-excess in surface snow along a traverse from Zhongshan station to
Dome A, East Antarctica, Earth and Planetary Science Letters, 414, 126–133, https://doi.org/10.1016/j.epsl.2015.01.014, 2015.

Parish, T. R. and Bromwich, D. H.: Continental-Scale Simulation of the Antarctic Katabatic Wind Regime, Journal of Climate,
4, 135–146, https://doi.org/10.1175/1520-0442(1991)004<0135:CSSOTA>2.0.CO;2, 1991.

1130   Parish, T. R. and Waight, K. T.: The Forcing of Antarctic Katabatic Winds, Monthly Weather Review, 115, 2214–2226,
https://doi.org/10.1175/1520-0493(1987)115<2214:TFOAKW>2.0.CO;2, 1987.

Pedro, J. B., Jochum, M., Buizert, C., He, F., Barker, S., and Rasmussen, S. O.: Beyond the bipolar seesaw: Toward a process
understanding of interhemispheric coupling, Quaternary Science Reviews, 192, 27–46,
https://doi.org/10.1016/j.quascirev.2018.05.005, 2018.

1135   Persson, A., Langen, P. L., Ditlevsen, P., and Vinther, B. M.: The influence of precipitation weighting on interannual variability
of stable water isotopes in Greenland, J. Geophys. Res., 116, D20120, https://doi.org/10.1029/2010JD015517, 2011.

Pietroni, I., Argentini, S., and Petenko, I.: One Year of Surface-Based Temperature Inversions at Dome C, Antarctica,
Boundary-Layer Meteorol, 150, 131–151, https://doi.org/10.1007/s10546-013-9861-7, 2014.

Rhodes, R. H., Faïn, X., Stowasser, C., Blunier, T., Chappellaz, J., McConnell, J. R., Romanini, D., Mitchell, L. E., and Brook,
E. J.: Continuous methane measurements from a late Holocene Greenland ice core: Atmospheric and in-situ signals, Earth and
Planetary Science Letters, 368, 9–19, https://doi.org/10.1016/j.epsl.2013.02.034, 2013.

Ritz, C.: Time dependent boundary conditions for calculation of temperature fields in ice sheets, IAHS Publ, 170, 207–216,
1987.

Rubino, M., Etheridge, D. M., Thornton, D. P., Howden, R., Allison, C. E., Francey, R. J., Langenfelds, R. L., Steele, L. P.,
Trudinger, C. M., Spencer, D. A., Curran, M. A. J., van Ommen, T. D., and Smith, A. M.: Revised records of atmospheric
trace gases CO_2, CH_4, N_2O, and $\delta^{13}C$-CO_2 over the last 2000 years from Law Dome, Antarctica, Earth System Science Data,
11, 473–492, https://doi.org/10.5194/essd-11-473-2019, 2019.

Servettaz, A. P. M., Orsi, A. J., Curran, M. A. J., Moy, A. D., Landais, A., Agosta, C., Winton, V. H. L., Touzeau, A.,
McConnell, J. R., Werner, M., and Baroni, M.: Snowfall and Water Stable Isotope Variability in East Antarctica Controlled
by Warm Synoptic Events, J. Geophys. Res. Atmos., 125, https://doi.org/10.1029/2020JD032863, 2020.

Severinghaus, J. and Battle, M.: Fractionation of gases in polar ice during bubble close-off: New constraints from firn air Ne,
Kr and Xe observations, Earth and Planetary Science Letters, 244, 474–500, https://doi.org/10.1016/j.epsl.2006.01.032, 2006.

Severinghaus, J. P., Grachev, A., and Battle, M.: Thermal fractionation of air in polar firn by seasonal temperature gradients:
THERMAL FRACTIONATION OF AIR, Geochem. Geophys. Geosyst., 2, n/a-n/a, https://doi.org/10.1029/2000GC000146,
2001.

Severinghaus, J. P., Grachev, A., Luz, B., and Caillon, N.: A method for precise measurement of argon 40/36 and krypton/argon
ratios in trapped air in polar ice with applications to past firn thickness and abrupt climate change in Greenland and at Siple
Dome, Antarctica, Geochimica et Cosmochimica Acta, 67, 325–343, https://doi.org/10.1016/S0016-7037(02)00965-1, 2003.

Sigl, M., McConnell, J. R., Layman, L., Maselli, O., McGwire, K., Pasteris, D., Dahl-Jensen, D., Steffensen, J. P., Vinther, B.,
Edwards, R., Mulvaney, R., and Kipfstuhl, S.: A new bipolar ice core record of volcanism from WAIS Divide and NEEM and
implications for climate forcing of the last 2000 years, Journal of Geophysical Research: Atmospheres, 118, 1151–1169,
https://doi.org/10.1029/2012JD018603, 2013.

Sigl, M., McConnell, J. R., Toohey, M., Curran, M., Das, S. B., Edwards, R., Isaksson, E., Kawamura, K., Kipfstuhl, S.,
Krüger, K., Layman, L., Maselli, O. J., Motizuki, Y., Motoyama, H., Pasteris, D. R., and Severi, M.: Insights from Antarctica
on volcanic forcing during the Common Era, Nature Clim Change, 4, 693–697, https://doi.org/10.1038/nclimate2293, 2014.

Sigl, M., Winstrup, M., McConnell, J. R., Welten, K. C., Plunkett, G., Ludlow, F., Büntgen, U., Caffee, M., Chellman, N.,
Dahl-Jensen, D., Fischer, H., Kipfstuhl, S., Kostick, C., Maselli, O. J., Mekhaldi, F., Mulvaney, R., Muscheler, R., Pasteris,
D. R., Pilcher, J. R., Salzer, M., Schüpbach, S., Steffensen, J. P., Vinther, B. M., and Woodruff, T. E.: Timing and climate
forcing of volcanic eruptions for the past 2,500 years, Nature, 523, 543–549, https://doi.org/10.1038/nature14565, 2015a.

Sigl, M., Winstrup, M., McConnell, J. R., Welten, K. C., Plunkett, G., Ludlow, F., Büntgen, U., Caffee, M., Chellman, N.,
Dahl-Jensen, D., Fischer, H., Kipfstuhl, S., Kostick, C., Maselli, O. J., Mekhaldi, F., Mulvaney, R., Muscheler, R., Pasteris,
D. R., Pilcher, J. R., Salzer, M., Schüpbach, S., Steffensen, J. P., Vinther, B. M., and Woodruff, T. E.: Timing and climate
forcing of volcanic eruptions for the past 2,500 years, Nature, 523, 543–549, https://doi.org/10.1038/nature14565, 2015b.

Sigl, M., Fudge, T., Winstrup, M., Cole-Dai, J., Ferris, D., Mcconnell, J., Taylor, K., Welten, K., Woodruff, T., Adolphi, F.,
Bisiaux, M., Brook, E., Buizert, C., Caffee, M., Dunbar, N., Edwards, R., Geng, L., Iverson, N., Koffman, B., Layman, L.,
Maselli, O., Mcgwire, K., Muscheler, R., Nishiizumi, K., Pasteris, D., Rhodes, R., and Sowers, T.: The WAIS Divide deep ice
core WD2014 chronology - Part 2: Annual-layer counting (0-31 ka BP), Clim. Past, 19, 2016a.

Climate
of the Past

Discussions

Sigl, M., Fudge, T., Winstrup, M., Cole-Dai, J., Ferris, D., Mcconnell, J., Taylor, K., Welten, K., Woodruff, T., Adolphi, F., Bisiaux, M., Brook, E., Buizert, C., Caffee, M., Dunbar, N., Edwards, R., Geng, L., Iverson, N., Koffman, B., Layman, L., 1180 Maselli, O., Mcgwire, K., Muscheler, R., Nishiizumi, K., Pasteris, D., Rhodes, R., and Sowers, T.: The WAIS Divide deep ice core WD2014 chronology - Part 2: Annual-layer counting (0-31 ka BP), Clim. Past, 19, 2016b.

Sowers, T., Bender, M., Raynaud, D., and Korotkevich, Y. S.: δ15N of N2 in air trapped in polar ice: A tracer of gas transport in the firn and a possible constraint on ice age-gas age differences, Journal of Geophysical Research: Atmospheres, 97, 15683–15697, https://doi.org/10.1029/92JD01297, 1992.

1185 Steen-Larsen, H. C., Masson-Delmotte, V., Hirabayashi, M., Winkler, R., Satow, K., Prié, F., Bayou, N., Brun, E., Cuffey, K. M., Dahl-Jensen, D., Dumont, M., Guillevic, M., Kipfstuhl, S., Landais, A., Popp, T., Risi, C., Steffen, K., Stenni, B., and Sveinbjörnsdottír, A. E.: What controls the isotopic composition of Greenland surface snow?, Climate of the Past, 10, 377–392, https://doi.org/10.5194/CP-10-377-2014, 2014.

Steig, E. J., Morse, D. L., Waddington, E. D., Stuiver, M., Grootes, P. M., Mayewski, P. A., Twickler, M. S., and Whitlow, S. 1190 I.: Wisconsinan and Holocene Climate History from an Ice Core at Taylor Dome, Western Ross Embayment, Antarctica, Geografiska Annaler: Series A, Physical Geography, 82, 213–235, https://doi.org/10.1111/j.0435-3676.2000.00122.x, 2000.

Steig, E. J., Ding, Q., White, J. W. C., Küttel, M., Rupper, S. B., Neumann, T. A., Neff, P. D., Gallant, A. J. E., Mayewski, P. A., Taylor, K. C., Hoffmann, G., Dixon, D. A., Schoenemann, S. W., Markle, B. R., Fudge, T. J., Schneider, D. P., Schauer, A. J., Teel, R. P., Vaughn, B. H., Burgener, L., Williams, J., and Korotkikh, E.: Recent climate and ice-sheet changes in West 1195 Antarctica compared with the past 2,000 years, Nature Geosci, 6, 372–375, https://doi.org/10.1038/ngeo1778, 2013.

Stenni, B., Scarchilli, C., Masson-Delmotte, V., Schlosser, E., Ciardini, V., Dreossi, G., Grigioni, P., Bonazza, M., Cagnati, A., Karlicek, D., Risi, C., Udisti, R., and Valt, M.: Three-year monitoring of stable isotopes of precipitation at Concordia Station, East Antarctica, The Cryosphere, 10, 2415–2428, https://doi.org/10.5194/tc-10-2415-2016, 2016.

Stenni, B., Curran, M. A. J., Abram, N. J., Orsi, A. J., Goursaud, S., Masson-Delmotte, V., Neukom, R., Goosse, H., Divine, 1200 D., van Ommen, T., Steig, E. J., Dixon, D. A., Thomas, E. R., Bertler, N. A. N., Isaksson, E., Ekaykin, A., Werner, M., and Frezzotti, M.: Antarctic climate variability on regional and continental scales over the last 2000 years, Clim. Past, 13, 1609–1634, https://doi.org/10.5194/cp-13-1609-2017, 2017.

Stokes, C. R., Abram, N. J., Bentley, M. J., Edwards, T. L., England, M. H., Foppert, A., Jamieson, S. S. R., Jones, R. S., King, M. A., Lenaerts, J. T. M., Medley, B., Miles, B. W. J., Paxman, G. J. G., Ritz, C., van de Flierdt, T., and Whitehouse, P. L.: 1205 Response of the East Antarctic Ice Sheet to past and future climate change, Nature, 608, 275–286, https://doi.org/10.1038/s41586-022-04946-0, 2022.

Tierney, J. E., Abram, N. J., Anchukaitis, K. J., Evans, M. N., Giry, C., Kilbourne, K. H., Saenger, C. P., Wu, H. C., and Zinke, J.: Tropical sea surface temperatures for the past four centuries reconstructed from coral archives, Paleoceanography, 30, 226–252, https://doi.org/10.1002/2014PA002717, 2015.

1210 Turner, J., Phillips, T., Thamban, M., Rahaman, W., Marshall, G. J., Wille, J. D., Favier, V., Winton, V. H. L., Thomas, E., Wang, Z., Broeke, M. van den, Hosking, J. S., and Lachlan-Cope, T.: The Dominant Role of Extreme Precipitation Events in Antarctic Snowfall Variability, Geophysical Research Letters, 46, 3502–3511, https://doi.org/10.1029/2018GL081517, 2019.

Uemura, R., Matsui, Y., Yoshimura, K., Motoyama, H., and Yoshida, N.: Evidence of deuterium excess in water vapor as an indicator of ocean surface conditions, J. Geophys. Res., 113, D19114, https://doi.org/10.1029/2008JD010209, 2008.

1215   Uemura, R., Yonezawa, N., Yoshimura, K., Asami, R., Kadena, H., Yamada, K., and Yoshida, N.: Factors controlling isotopic composition of precipitation on Okinawa Island, Japan: Implications for paleoclimate reconstruction in the East Asian Monsoon region, Journal of Hydrology, 475, 314–322, https://doi.org/10.1016/j.jhydrol.2012.10.014, 2012.

Van Liefferinge, B., Taylor, D., Tsutaki, S., Fujita, S., Gogineni, P., Kawamura, K., Matsuoka, K., Moholdt, G., Oyabu, I., Abe-Ouchi, A., Awasthi, A., Buizert, C., Gallet, J., Isaksson, E., Motoyama, H., Nakazawa, F., Ohno, H., O'Neill, C., Pattyn,
1220   F., and Sugiura, K.: Surface Mass Balance Controlled by Local Surface Slope in Inland Antarctica: Implications for Ice-Sheet Mass Balance and Oldest Ice Delineation in Dome Fuji, Geophysical Research Letters, 48, https://doi.org/10.1029/2021GL094966, 2021.

Vihma, T., Tuovinen, E., and Savijärvi, H.: Interaction of katabatic winds and near-surface temperatures in the Antarctic, Journal of Geophysical Research: Atmospheres, 116, https://doi.org/10.1029/2010JD014917, 2011.

1225   Wang, W. L. and Warner, R. C.: Modelling of anisotropic ice flow in Law Dome, East Antarctica, Ann. Glaciol., 29, 184–190, https://doi.org/10.3189/172756499781820932, 1999.

Werner, M., Mikolajewicz, U., Heimann, M., and Hoffmann, G.: Borehole versus isotope temperatures on Greenland: Seasonality does matter, Geophysical Research Letters, 27, 723–726, https://doi.org/10.1029/1999GL006075, 2000.

Witrant, E., Martinerie, P., Hogan, C., Laube, J. C., Kawamura, K., Capron, E., Montzka, S. A., Dlugokencky, E. J., Etheridge,
1230   D., Blunier, T., and Sturges, W. T.: A new multi-gas constrained model of trace gas non-homogeneous transport in firn: evaluation and behaviour at eleven polar sites, Atmospheric Chemistry and Physics, 12, 11465–11483, https://doi.org/10.5194/acp-12-11465-2012, 2012.

Wolff, E. W., Barbante, C., Becagli, S., Bigler, M., Boutron, C. F., Castellano, E., de Angelis, M., Federer, U., Fischer, H., Fundel, F., Hansson, M., Hutterli, M., Jonsell, U., Karlin, T., Kaufmann, P., Lambert, F., Littot, G. C., Mulvaney, R.,
1235   Röthlisberger, R., Ruth, U., Severi, M., Siggaard-Andersen, M. L., Sime, L. C., Steffensen, J. P., Stocker, T. F., Traversi, R., Twarloh, B., Udisti, R., Wagenbach, D., and Wegner, A.: Changes in environment over the last 800,000 years from chemical analysis of the EPICA Dome C ice core, Quaternary Science Reviews, 29, 285–295, https://doi.org/10.1016/j.quascirev.2009.06.013, 2010.

Wright, N. M., Krause, C. E., Phipps, S. J., Boschat, G., and Abram, N. J.: Influence of long-term changes in solar irradiance
1240   forcing on the Southern Annular Mode, Climate of the Past, 18, 1509–1528, https://doi.org/10.5194/cp-18-1509-2022, 2022.

Xiao, C., Ding, M., Masson-Delmotte, V., Zhang, R., Jin, B., Ren, J., Li, C., Werner, M., Wang, Y., Cui, X., and Wang, X.: Stable isotopes in surface snow along a traverse route from Zhongshan station to Dome A, East Antarctica, Clim Dyn, 41, 2427–2438, https://doi.org/10.1007/s00382-012-1580-0, 2013.

Yokoyama, Y., Anderson, J. B., Yamane, M., Simkins, L. M., Miyairi, Y., Yamazaki, T., Koizumi, M., Suga, H., Kusahara,
1245   K., Prothro, L., Hasumi, H., Southon, J. R., and Ohkouchi, N.: Widespread collapse of the Ross Ice Shelf during the late Holocene, Proc. Natl. Acad. Sci. U.S.A., 113, 2354–2359, https://doi.org/10.1073/pnas.1516908113, 2016.